
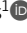


**ARTICLE**

Excitation–Contraction Coupling

# A mathematical model to quantify RYR Ca<sup>2+</sup> leak and associated heat production in resting human skeletal muscle fibers

 Christopher J. Barclay<sup>1</sup>  and Bradley S. Launikonis<sup>1</sup> 

Cycling of Ca<sup>2+</sup> between the sarcoplasmic reticulum (SR) and myoplasm is an important component of skeletal muscle resting metabolism. As part of this cycle, Ca<sup>2+</sup> leaks from the SR into the myoplasm and is pumped back into the SR using ATP, which leads to the consumption of O<sub>2</sub> and generation of heat. Ca<sup>2+</sup> may leak through release channels or ryanodine receptors (RYRs). RYR Ca<sup>2+</sup> leak can be monitored in a skinned fiber preparation in which leaked Ca<sup>2+</sup> is pumped into the t-system and measured with a fluorescent dye. However, accurate quantification faces a number of hurdles. To overcome them, we developed a mathematical model of Ca<sup>2+</sup> movement in these preparations. The model incorporated Ca<sup>2+</sup> pumps that move Ca<sup>2+</sup> from the myoplasm to the SR and from the junctional space (JS) to the t-system, Ca<sup>2+</sup> buffering by EGTA in the JS and myoplasm and by buffers in the SR, and Ca<sup>2+</sup> leaks from the SR into the JS and myoplasm and from the t-system into the myoplasm. The model accurately simulated Ca<sup>2+</sup> uptake into the t-system, the relationship between myoplasmic [Ca<sup>2+</sup>] and steady-state t-system [Ca<sup>2+</sup>], and the effect of blocking RYR Ca<sup>2+</sup> leak on t-system Ca<sup>2+</sup> uptake. The magnitude of the leak through the RYRs would contribute ~5% of the resting heat production of human muscle. In normal resting fibers, RYR Ca<sup>2+</sup> leak makes a small contribution to resting metabolism. RYR-focused pathologies have the potential to increase RYR Ca<sup>2+</sup> leak and the RYR leak component of resting metabolism.

## Introduction

Cycling of calcium ions (Ca<sup>2+</sup>) between the sarcoplasmic reticulum (SR) and the myoplasm is central to excitation–contraction coupling in muscle: release of Ca<sup>2+</sup> into the myoplasm and its subsequent binding to sites on troponin C (TnC) initiate and maintain contraction, and removal of Ca<sup>2+</sup> from the myoplasm initiates relaxation. However, Ca<sup>2+</sup> cycling is important even in unstimulated or resting muscle and contributes to resting metabolism. In resting muscle, there appears to be a steady leak of Ca<sup>2+</sup> from the SR into the myoplasm that is balanced by removal of Ca<sup>2+</sup> from the myoplasm into the SR via the SR Ca<sup>2+</sup> pump (Chinet et al., 1992). The concentration of free, or unbound, Ca<sup>2+</sup> in the myoplasm is steady in resting muscle (Konishi and Watanabe, 1995), indicating that the rate at which Ca<sup>2+</sup> leaks into the myoplasm is equal to the rate at which it is pumped into the SR. The SR Ca<sup>2+</sup> pump (SERCA) is powered by ATP and, in a

metabolic steady state, ATP is replenished by mitochondrial oxidative phosphorylation at the same rate at which it is used. The ATP regenerating processes produce heat, and the heat associated with SERCA activity accounts for about one-quarter of the heat produced by resting mouse skeletal muscles (Chinet et al., 1992).

Two Ca<sup>2+</sup> leak processes, that are not mutually exclusive, have been proposed. First, Ca<sup>2+</sup> can leak from the SR through the Ca<sup>2+</sup> release channels or ryanodine receptors (RYRs; Cully et al., 2016). The importance of this pathway is that the leakiness of RYRs has been shown to vary across a range of naturally occurring variants of RYRs, perhaps most strikingly in the highly modified heater muscles of some fish (Morrissette et al., 2003), and to be associated with pathological conditions, such as malignant hyperthermia (Cully et al., 2018). Second, Ca<sup>2+</sup> can leak

<sup>1</sup>School of Biomedical Sciences, University of Queensland, Queensland, Australia.

Correspondence to Christopher J. Barclay: [c.barclay@uq.edu.au](mailto:c.barclay@uq.edu.au)

This work is part of a special issue on excitation–contraction coupling.

© 2022 Barclay and Launikonis. This article is distributed under the terms of an Attribution–Noncommercial–Share Alike–No Mirror Sites license for the first six months after the publication date (see <http://www.rupress.org/terms/>). After six months it is available under a Creative Commons License (Attribution–Noncommercial–Share Alike 4.0 International license, as described at <https://creativecommons.org/licenses/by-nc-sa/4.0/>).

from the SR into the myoplasm via a mechanism independent of RYRs but that involves SERCA (Simonides and Van Hardeveld, 1988; Macdonald and Stephenson, 2001; Lamboley et al., 2014). The focus of the current study is the first of these mechanisms,  $\text{Ca}^{2+}$  leak through the RYRs.

Launikonis and colleagues have developed a method to measure the rate of  $\text{Ca}^{2+}$  leak through the RYRs in unstimulated or resting muscle fibers (Cully et al., 2016; Cully et al., 2017; Cully et al., 2018). A skinned muscle fiber preparation is used in which at least some of the  $\text{Ca}^{2+}$  that leaks through the RYRs is pumped into the t-tubules, which are sealed from the extracellular space in this particular preparation and are loaded with a  $\text{Ca}^{2+}$ -sensitive dye. The inside of the fiber preparation is heavily buffered against changes in  $[\text{Ca}^{2+}]$  by the presence of EGTA. In the junctional space (JS) adjacent to the RYRs, the presence of EGTA attenuates changes in  $\text{Ca}^{2+}$  concentration due to RYR leaks so that the variation in the concentration of unbound  $\text{Ca}^{2+}$  in the JS ( $\text{Ca}_{\text{JS}}$ ) due to leaks is within the working range of the  $\text{Ca}^{2+}$  pump in the neighboring t-tubule membrane. In this way, the rate at which the pump (a plasma membrane  $\text{Ca}^{2+}$  ATPase [PMCA]) moves  $\text{Ca}^{2+}$  into the t-tubule reflects  $\text{Ca}_{\text{JS}}$  and thus the rate at which  $\text{Ca}^{2+}$  leaks through the RYRs. If  $\text{Ca}^{2+}$  leaks through the RYRs rapidly enough to raise  $\text{Ca}_{\text{JS}}$ , then the rate and extent of  $\text{Ca}^{2+}$  accumulation in the t-system will be increased. A key aspect of these experiments is that the RYR  $\text{Ca}^{2+}$  flux can be inhibited pharmacologically, using tetracaine. The magnitude of trans-RYR  $\text{Ca}^{2+}$  leak can then be inferred from the difference in the rate and extent of t-tubule  $\text{Ca}^{2+}$  accumulation before and after the inhibition (Cully et al., 2018). Those experiments indicate that there is a continual leak of  $\text{Ca}^{2+}$  through the RYR in unstimulated fibers of human skeletal muscle. However, the complexity of the experimental preparation makes it difficult to determine the magnitude of the RYR  $\text{Ca}^{2+}$  leak.

Specific aspects of the preparation and the experimental methods that complicate the relationship between RYR  $\text{Ca}^{2+}$  leak and t-tubule  $\text{Ca}^{2+}$  uptake are as follows: (1) the skinned fiber contains a high concentration of EGTA, which is used to control the myoplasmic  $\text{Ca}^{2+}$  concentration ( $\text{Ca}_{\text{M}}$ ) to match the range over which the PMCA functions. However, the buffering action of EGTA must also attenuate the increase in  $\text{Ca}_{\text{JS}}$  that occurs when  $\text{Ca}^{2+}$  leaks into the JS. (2) It is likely that there is a leak of  $\text{Ca}^{2+}$  from the t-system into the myoplasm (Cully et al., 2018; Meizoso-Huesca and Launikonis, 2021). In that case, the empirical relationship between the concentration of unbound  $\text{Ca}^{2+}$  in the t-system ( $\text{Ca}_{\text{T}}$ ) and  $\text{Ca}_{\text{JS}}$  reflects the combined characteristics of  $\text{Ca}^{2+}$  uptake by the PMCA and  $\text{Ca}^{2+}$  leak from the t-system. (3) JS volume ( $V_{\text{JS}}$ ) is small compared to that of the SR ( $V_{\text{SR}}$ ;  $V_{\text{JS}} < 0.1\% V_{\text{SR}}$ ; Eisenberg, 1983), so a leak of  $\text{Ca}^{2+}$  through the RYRs that makes only a small change in  $\text{Ca}_{\text{SR}}$  will produce a large change in the total  $\text{Ca}^{2+}$  concentration (i.e., free + bound to EGTA) in the JS. (4) The experimental protocol starts with emptying  $\text{Ca}^{2+}$  from the t-tubules and SR. It is not known whether the subsequent time course of SR filling, which in turn is likely to affect RYR leak, influences the time course of t-system  $\text{Ca}^{2+}$  accumulation.

One way of assessing how these aspects of the preparation and protocol influence the experimental results is to use a

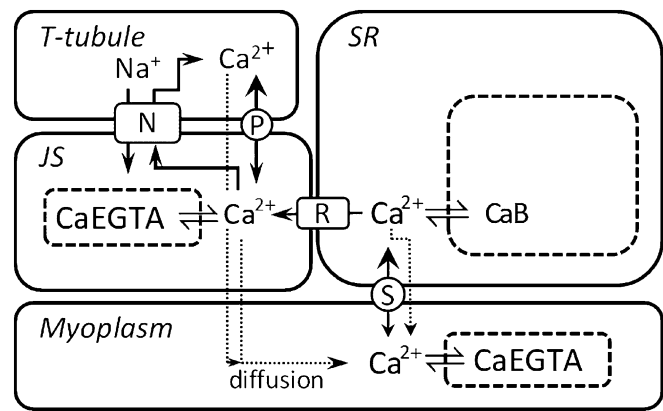


Figure 1. **Schematic of experimental fiber model.** The model includes four physical spaces, the myoplasm, SR, JS, and t-tubule. In the SR,  $\text{Ca}^{2+}$  is in equilibrium with buffers (B), which includes  $\text{Ca}_{\text{sq}}$ . In the myoplasm and JS,  $\text{Ca}^{2+}$  is in equilibrium with EGTA.  $\text{Ca}^{2+}$  movements were constrained as follows: (1)  $\text{Ca}^{2+}$  enters the SR only from the myoplasm via SERCA (labeled S); (2)  $\text{Ca}^{2+}$  enters the t-tubule only from the JS and via PMCA (P) and NCX (N); (3)  $\text{Ca}^{2+}$  enters the JS by leak from the SR (through the RYR [R]), potentially from NCX working in reverse and from dissociation of  $\text{Ca}^{2+}$  bound to EGTA; (4)  $\text{Ca}^{2+}$  can enter the myoplasm by leaking from the SR or the t-system and by diffusive exchange with the JS. The relative sizes of the spaces in the diagram do not reflect the actual relative volumes in a fiber.

mathematical model of the preparation. The purpose of the current study was to develop a model that could be used to quantify the leak of  $\text{Ca}^{2+}$  from the SR through the RYRs, to identify factors that influence t-tubule  $\text{Ca}^{2+}$  accumulation, and to estimate the contribution of trans-RYR  $\text{Ca}^{2+}$  flux to the metabolism of resting muscle.

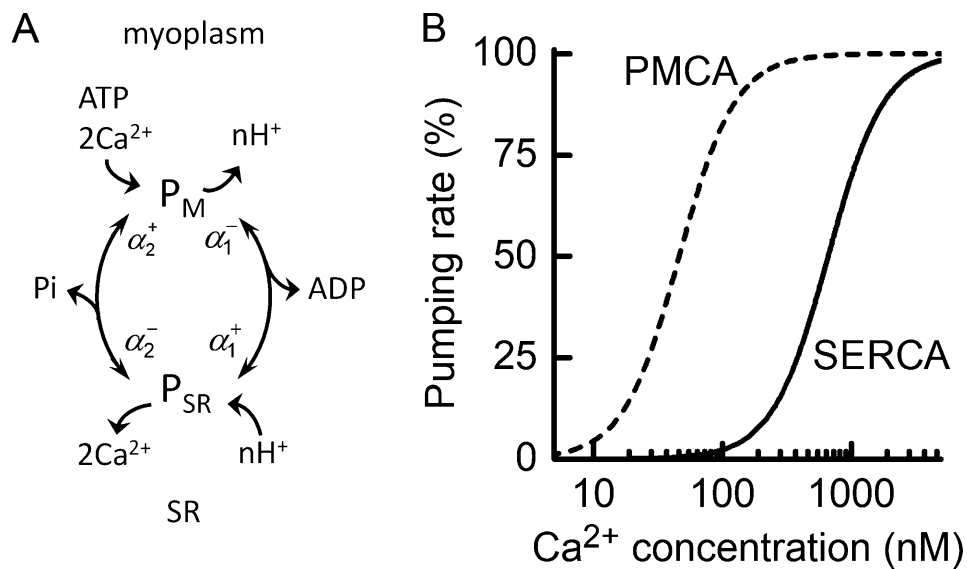
## Materials and methods

### Overview of the model

The model describes the movements of  $\text{Ca}^{2+}$  among the SR, t-tubule, JS, and myoplasm and is illustrated in Fig. 1. The sub-cellular system that was modeled included seven compartments that  $\text{Ca}^{2+}$  can occupy, four of which are physically discrete spaces and three of which are molecular compartments (i.e.,  $\text{Ca}^{2+}$  in equilibrium with buffer molecules). The compartments are (1) t-tubules, (2) SR, (3) JS (i.e., region between t-tubule and SR  $\text{Ca}^{2+}$  release channels), (4) myoplasm, (5) EGTA in the myoplasm, (6) EGTA in the JS, and (7)  $\text{Ca}^{2+}$  buffers, including calsequestrin ( $\text{Ca}_{\text{sq}}$ ), in the SR.

### Mathematical description of the model

The rates of change in concentration of  $\text{Ca}^{2+}$  in each of the compartments, taking into account the constraints on  $\text{Ca}^{2+}$  movements described in the legend of Fig. 1 and the relative volumes of the physical compartments, were described by ordinary differential equations. The equations incorporated  $\text{Ca}^{2+}$  movements due to (1) ATP-dependent pumping of  $\text{Ca}^{2+}$  from the myoplasm into the SR via SERCA, (2) ATP-dependent pumping of  $\text{Ca}^{2+}$  from the JS into the t-tubules via PMCA, (3) exchange of  $\text{Na}^{+}$  and  $\text{Ca}^{2+}$  between the JS and t-tubule via the sodium/calcium exchanger (NCX), and (4) diffusive exchange of  $\text{Ca}^{2+}$



**Figure 2. Characteristics of Ca<sup>2+</sup> pumps used in model.** (A) Schematic of the two-state Ca<sup>2+</sup> pump model used for SERCA and PMCA. The model consists of two states, one on the myoplasmic side of the membrane (labeled P<sub>M</sub>), where Ca<sup>2+</sup> is collected, and one on the luminal side of the SR membrane for SERCA or t-tubular membrane for PMCA (P<sub>SR</sub>), where Ca<sup>2+</sup> is released. The diagram illustrates the forward and reverse rate constants for transitions between the states (α), Ca<sup>2+</sup> transport, H<sup>+</sup> countertransport, and hydrolysis of ATP to provide energy. The rate constants are functions of [ATP] and its metabolites and pH. (B) Dependence on [Ca<sup>2+</sup>] of Ca<sup>2+</sup> pumping rate of SERCA and PMCA. Curves constructed using the model showing relationship between relative rate of Ca<sup>2+</sup> pumping (% maximum rate) and [Ca<sup>2+</sup>] using the K<sub>d</sub> values for Ca<sup>2+</sup> dissociation on the myoplasmic side as applied in the current analysis. The maximal rates of pumping (with concentrations expressed relative to myoplasmic water volume; see Table 3) were SERCA, 711 μM s<sup>-1</sup>; and PMCA, 0.15 μM s<sup>-1</sup>. Note that expressed relative to JS volume, PMCA maximal Ca<sup>2+</sup> pumping rate was 705 μM s<sup>-1</sup>. The Ca<sub>50</sub> values were SERCA, 700 nM; and PMCA, 46 nM.

between the JS and myoplasm. The concentrations of unbound Ca<sup>2+</sup> in the myoplasm and JS were determined from the equilibrium between Ca<sup>2+</sup> and EGTA, and that in the SR from the equilibrium between Ca<sup>2+</sup> and the SR buffers. The equation formulation ensured that total Ca<sup>2+</sup> in the system remained constant.

To provide the model with the complexity and responsiveness to local conditions that is evident in physiological systems, where possible mechanistic descriptions of model components were used. Models for SERCA and PMCA were taken from models described and validated in the literature. Cully et al. (2018) showed that t-system Ca<sup>2+</sup> accumulation in human fibers was unaffected by pharmacological inhibition of NCX. Therefore, NCX was not incorporated into the final model. Temperature-sensitive model parameters obtained from the literature were adjusted to values appropriate for a temperature of 25°C, similar to that used for the muscle fiber experiments, assuming a Q<sub>10</sub> (change in rate for a 10°C change in temperature) of 2.

### Model components

#### SR Ca<sup>2+</sup> pump (SERCA)

In each pump cycle, SERCA moves two Ca<sup>2+</sup> from the myoplasm up a concentration gradient into the SR at the expense of one ATP (Weber et al., 1966; Makinose and Hasselbach, 1971). The pump was modeled as described by Tran et al. (2009). Those authors derived a 2-state model (Fig. 2 A) from a 12-state biochemical model. In reducing the model to 2 states, the relevant complexity of the 12-state model was maintained in that the apparent rate constants describing the forward and reverse

transitions between the 2 states depend on pH, the concentrations of ATP and its hydrolysis products, and [Ca<sup>2+</sup>] on both sides of the SR membrane (see Appendix 1). The model is thermodynamically constrained; that is, the rate of Ca<sup>2+</sup> pumping depends on the difference in free energy produced by ATP hydrolysis (ΔG<sub>ATP</sub>) and the free energy generated by the Ca<sup>2+</sup> concentration gradient (ΔG<sub>Ca</sub>). The equations describing the pumping rate are given in Appendix 1.

To align the SERCA model with human skeletal muscle, appropriate values for the pump's concentration and Ca<sup>2+</sup> sensitivity were determined. Sensitivity of the pump to Ca<sup>2+</sup> is quantified by its Ca<sub>50</sub> value (the Ca<sub>M</sub> at which the pump rate is 50% of its maximum). A constraint on the sensitivity is that the rate of Ca<sup>2+</sup> pumping when Ca<sub>M</sub> is at resting levels should not result in SERCA producing heat from oxidative regeneration of ATP consumed by the pump at a rate greater than the experimentally determined Ca<sup>2+</sup>-related heat output in resting muscles. SERCA has been reported to account for ~25% of the resting metabolism of mouse slow-twitch muscle (Chinet et al., 1992) and 20% of rat fast-twitch muscle (Simonides and Van Hardeveld, 1988), but there are also much lower estimates (e.g., 3–5%; Clausen et al., 1991; Rolfe and Brown, 1997). The rate of heat output from noncontracting human forearm muscles is 0.6 W kg<sup>-1</sup> (Table 1), or 600 mW kg<sup>-1</sup>, so if it is assumed that 25% of this is due to Ca<sup>2+</sup> cycling via SERCA, then ATP use by the pump would produce heat at 0.25 × 600 = 150 mW kg<sup>-1</sup>.

A Ca<sub>50</sub> value that is consistent with this rate of heat production can be calculated as follows. In resting skeletal muscle, Ca<sub>M</sub> is in the range 0.05–0.1 μM (for a review, see Konishi, 1998). At 25°C, the maximum rate of ATP breakdown by

Table 1. **Rate of heat output from resting human skeletal muscle**

Forearm resting VO <sub>2</sub> at 35°C	2.2	ml (liter muscle) <sup>-1</sup> min <sup>-1</sup>	Zurlo et al. (1990)
Rate of muscle heat production at 35°C	46	J (liter muscle) <sup>-1</sup> min <sup>-1</sup>	Assuming 20.9 kJ (liter O <sub>2</sub> ) <sup>-1</sup>
Express in W (kg muscle) <sup>-1</sup>	0.73	W (kg muscle) <sup>-1</sup>	Muscle density, 1.06 kg liter <sup>-1</sup>
Express in W (kg myoplasmic water) <sup>-1</sup>	1.2	W (kg myoplasmic H <sub>2</sub> O) <sup>-1</sup>	Whole muscle volume = 1.45 × myoplasmic H <sub>2</sub> O volume (Table 3)
Rate of muscle heat production at 25°C	0.60	W (kg myoplasmic H <sub>2</sub> O) <sup>-1</sup>	Q <sub>10</sub> = 2 (Barclay et al., 2009)

SERCA in human type 2 fibers is 355 μM s<sup>-1</sup> (Table 2). The heat associated with Ca<sup>2+</sup> cycling in resting muscle arises from oxidative regeneration of ATP; if glucose is the substrate (molar enthalpy change, 2,802 mJ μmol<sup>-1</sup>; Kabo et al., 2013) and 38 ATP are generated per glucose (for a review, see Barclay and Loisel, 2020), then the heat produced is 2,802/38 = 74 mJ (μmol ATP)<sup>-1</sup>. Assuming a sigmoidal dependence of rate of Ca<sup>2+</sup> pumping on Ca<sub>M</sub> with a slope of 2 (Fig. 2 B), Ca<sub>M</sub> of 0.05 μM in resting fast-twitch muscle and muscle density of 1.06 kg liter<sup>-1</sup>, then the Ca<sup>2+</sup>-related rate of heat production (Q; mW kg<sup>-1</sup>) is given by

$$Q = \frac{0.05^2}{0.05^2 + Ca_{50}^2} \cdot \frac{355.74}{1.06} \quad (1)$$

Setting Q to 150 mW kg<sup>-1</sup> and solving for Ca<sub>50</sub> gives 0.66 μM. This is probably a lower limit, because Ca<sub>50</sub> would be greater if resting Ca<sub>M</sub> was >50 nM. For the current study, Ca<sub>50</sub><sup>SERCA</sup> was set to 0.7 μM, which satisfies Eq. 1 and is comparable to estimates for other mammalian fast-twitch muscles (0.3 μM, Vilsen and Andersen, 1992; 0.62 μM, Cantilina et al., 1993).

The concentration of SERCA in human skeletal muscle was estimated using the maximal turnover rate for individual pumps under cellular conditions applicable to the current experimental preparation, and an estimate of the absolute maximum rate of Ca<sup>2+</sup> pumping (M<sub>Max</sub><sup>SERCA</sup>) was calculated using measurements of

Table 2. **Estimate of maximum rate of SR Ca<sup>2+</sup> pumping in intact fast-twitch human muscle fibers**

Variable	Value
Isometric ATP turnover <sup>a</sup>	2,333 μM s <sup>-1</sup>
Fraction of ATP turnover by Ca pump <sup>b</sup>	0.35
ATP turnover for Ca pumping at 37°C	817 μM s <sup>-1</sup>
ATP turnover for Ca pumping at 25°C <sup>c</sup>	355 μM s <sup>-1</sup>
Maximum rate of Ca uptake at 25°C <sup>d</sup>	711 μM s <sup>-1</sup>

<sup>a</sup>Expressed relative to myoplasmic H<sub>2</sub>O volume; converted from 140 mM min<sup>-1</sup> in sustained maximal contraction at 37°C (for details, see Barclay, 2017).

<sup>b</sup>From data for type 2A human fibers (Szentesi et al., 2001) and other mammalian muscles (Barclay et al., 2007).

<sup>c</sup>Assumed Q<sub>10</sub> = 2 (Barclay, 2012).

<sup>d</sup>Two Ca<sup>2+</sup> translocated for each ATP-splitting cycle (Weber et al., 1966).

energy turnover in human muscle fibers (Table 2). At the fiber level, the maximum rate of Ca<sup>2+</sup> pumping M<sub>Max</sub><sup>SERCA</sup> (μM s<sup>-1</sup>) is the product of the turnover rate of individual pumps (γ, s<sup>-1</sup>), the Ca<sup>2+</sup>/ATP stoichiometry (n<sub>SERCA</sub>), and pump concentration (c<sub>SERCA</sub>, μM):

$$M_{Max}^{SERCA} = c_{SERCA} \cdot n_{SERCA} \cdot \gamma \quad (2)$$

For SERCA, γ is ~6 s<sup>-1</sup> at 25°C (calculated from data in Lytton et al., 1992; Cantilina et al., 1993; Fortea et al., 2001). M<sub>Max</sub><sup>SERCA</sup> was taken to be 711 μM s<sup>-1</sup> (Table 2). Setting n<sub>SERCA</sub> = 2 and rearranging Eq. 2, c<sub>SERCA</sub> = 711 μM s<sup>-1</sup> / (2 × 6 s<sup>-1</sup>) = 59 μM (expressed relative to myoplasmic water volume). This compares favorably with values for fast-twitch muscles of other mammalian species. Baylor et al. (1983) calculated a pump concentration of 69 μM for rabbit fast-twitch muscle, and the data presented by Ferguson and Franzini-Armstrong (1988) (their Table 2) can be used to calculate a value of 68 μM for guinea pig fast-twitch muscle.

**Ca<sup>2+</sup>-cycling component of resting metabolism constrains the magnitude of SR Ca<sup>2+</sup> leak.** There is evidence that Ca<sup>2+</sup> leaks into the myoplasm from the SR via mechanisms in addition to RYR Ca<sup>2+</sup> leak. Ca<sup>2+</sup> leaks from the SR, even with the RYRs blocked, and at least part of this leak involves SERCA itself (Simonides and Van Hardeveld, 1988; Macdonald and Stephenson, 2001). A passive, concentration gradient-driven leak from the SR into the myoplasm, with a rate constant k<sub>Leak</sub><sup>SR</sup>, was incorporated into the model. The magnitude of Ca<sup>2+</sup> leak, by all mechanisms, from the SR into the myoplasm of resting muscle can be estimated from the energy expenditure of SERCA in resting muscle. Assuming that Ca<sup>2+</sup> cycling accounts for a heat production of 150 mW kg<sup>-1</sup>, as calculated above, and that the energy equivalent of ATP turnover is 74 mJ μmol<sup>-1</sup> (see above), then SERCA-related ATP turnover would be 150 mJ s<sup>-1</sup> kg<sup>-1</sup> / 74 mJ μmol<sup>-1</sup> ≈ 2.0 μmol kg<sup>-1</sup> s<sup>-1</sup>, and the rate of Ca<sup>2+</sup> pumping would be 4 μmol kg<sup>-1</sup> s<sup>-1</sup>. Taking into account of the relative volumes of the myoplasm and SR (Table 3), this uptake rate corresponds to Ca<sup>2+</sup> exiting the SR at 69 / 3.8 × 4 = 73 μM s<sup>-1</sup> with respect to SR volume. If Ca<sub>SR</sub> at rest is 400 μM (Sztretye et al., 2011b; Manno et al., 2013), this rate of loss is consistent with a rate constant of 73 μM s<sup>-1</sup> / 400 μM = 0.18 s<sup>-1</sup>. This represents the total SR Ca<sup>2+</sup> cycling, including leaks via RYRs and any other sources. k<sub>Leak</sub><sup>SR</sup> will, therefore, be 0.18 - k<sub>Leak</sub><sup>RYR</sup> s<sup>-1</sup>, where k<sub>Leak</sub><sup>RYR</sup> is the rate constant for Ca<sup>2+</sup> efflux from the SR through the RYRs.

### Plasma membrane Ca<sup>2+</sup> pump (PMCA)

It was assumed that the pump responsible for moving Ca<sup>2+</sup> into the t-tubule system is of the PMCA family (Cully et al., 2012). PMCA has a molecular structure similar to SERCA, with the addition of a region enabling kinetic modulation in vivo by calmodulin (Carafoli, 1991), and is localized to the junctional region of skeletal muscle (Sacchetto et al., 1996). The slope of the relationship between Ca<sup>2+</sup> pumping rate and [Ca<sup>2+</sup>] for PMCA is ~2 (Kosk-Kosicka and Inesi, 1985), indicative of the cooperative binding of 2 Ca<sup>2+</sup> in each pump cycle, which is consistent with direct measurements of the pump stoichiometry (Akyempon and Roufogalis, 1982; Valant and Haynes, 1993). It was therefore assumed that the mechanism of PMCA involves the binding



Table 3. **Volumes of muscle components and concentration conversion factors for human muscle**

Component	Relative volume (% fiber volume)	Comments
SR	3.8	Eisenberg (1983)
Mitochondria	5	Eisenberg (1983)
t-system	0.28	Eisenberg (1983)
JS	0.014	Estimated to be 5% of t-system volume (see text)
Myoplasmic water	69	Fraction of water in whole tissue that is inside fibers, excluding volumes occupied by SR, t-system, and JS
<b>Concentration conversion factors</b>		
Whole muscle (kg <sup>-1</sup> ) → fiber (liter <sup>-1</sup> )	1.18	
Whole muscle (kg <sup>-1</sup> ) → myoplasmic water (liter <sup>-1</sup> )	1.45	
Fiber (liter <sup>-1</sup> ) → myoplasmic water (liter <sup>-1</sup> )	1.23	

Other values required for calculations: whole muscle density, 1.05 kg liter<sup>-1</sup> (Segal et al., 1986) and protein density, 1.37 kg liter<sup>-1</sup> (Fischer et al., 2004; these values give ratio of wet mass/dry mass of whole muscle = 5); extracellular water, 12.5% of total muscle water (Sjogaard et al., 1985).

and transport of 2 Ca<sup>2+</sup> in each ATP-splitting cycle. The sensitivity of PMCA to Ca<sup>2+</sup> depends on calmodulin. In the absence of calmodulin, the pump's Ca<sub>50</sub> (Ca<sub>50</sub><sup>PMCA</sup>) is 5–10 μM, but this is reduced to <0.5 μM in the presence of calmodulin (Enyedi et al., 1993). EGTA, which was in the solutions used for the fiber studies on which the current analysis is based, also lowers Ca<sub>50</sub><sup>PMCA</sup> and to about the same extent as calmodulin (Schatzmann, 1973). The maximum pump turnover is similar for SERCA and PMCA. For instance, the maximum rates of ATP splitting by PMCA purified from human erythrocytes (Kosk-Kosicka and Inesi, 1985; Kosk-Kosicka and Bzdega, 1988; Enyedi et al., 1993), measured in the presence of calmodulin, are between 5 and 7 s<sup>-1</sup> at 25°C (assuming a Q<sub>10</sub> of 2). Therefore, as for SERCA, a maximum turnover of 6 s<sup>-1</sup> was used.

Given the structural and biochemical similarities between SERCA and PMCA, the same scheme (Fig. 2 A) was used to model both pumps (Sneyd, 2005; Croisier et al., 2013). Support for this approach can be seen in that reported relationships between the rate of ATP breakdown by PMCA and [Ca<sup>2+</sup>] can be described well using the model. For example, two empirical relationships between rate of ATP splitting and [Ca<sup>2+</sup>] are shown in Fig. 3, and both have been fitted with a curve calculated using the PMCA model equations, adjusting only the pump's Ca<sup>2+</sup> affinity. The form of the model predictions matches the data well, further supporting the idea that PMCA behaves in a manner consistent with cooperative binding of 2 Ca<sup>2+</sup> in each cycle. The dashed line in Fig. 3 shows the ATPase–Ca<sup>2+</sup> relationship produced when the model parameters were optimized to the human muscle fiber PMCA Ca<sup>2+</sup> accumulation data of Cully et al. (2018).

**Determinants of steady-state Ca<sub>T</sub>: thermodynamics or leak of Ca<sup>2+</sup> from t-system?** When the t-system fills with Ca<sup>2+</sup>, Ca<sub>T</sub> reaches a plateau after ~60–100 s (Cully et al., 2018). There are two potential causes of this phenomenon. First, the PMCA may reach its thermodynamic limit; that is, the plateau occurs when ΔG<sub>Ca</sub> rises sufficiently, as the concentration gradient increases,

to match ΔG<sub>ATP</sub>. An alternative, and not necessarily mutually exclusive, explanation is that there is passive leak of Ca<sup>2+</sup> out of the t-system, the rate of which depends on the [Ca<sup>2+</sup>] gradient between the t-tubule and the myoplasm. Each of these concepts is assessed in the following paragraphs. Predictions of the two models for limiting Ca<sub>M</sub> are compared to experimental data obtained in the presence of tetracaine (Fig. 4, circles); this is the

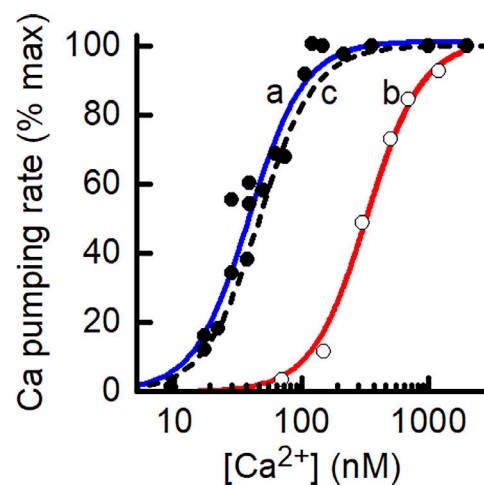


Figure 3. **Comparison of experimental and model-derived dependence of rate of PMCA Ca<sup>2+</sup> pumping on [Ca<sup>2+</sup>].** The PMCA model can replicate published ATPase data. The symbols are experimental data relating the rate of ATP splitting by PMCA as a function of [Ca<sup>2+</sup>] for different preparations of PMCA. Kosk-Kosicka and Inesi (1985; Fig. 3; used with permission from FEBS Letters). Filled circle, solubilized, purified PMCA from human erythrocytes, Ca<sub>50</sub>, 38 nM (Enyedi et al., 1993; Fig. 5); open circle, microsomal vesicles containing a human PMCA-derived construct, Ca<sub>50</sub>, 332 nM. The curves (a [blue] and b [red]) drawn through the data are the least-squares fit of the PMCA model used in the current study to the experimental data, adjusting only the value of PMCA Ca<sup>2+</sup> affinity. The dashed black line (c) shows the relationship used for analysis of Ca<sup>2+</sup> leak in the skinned fiber preparation.

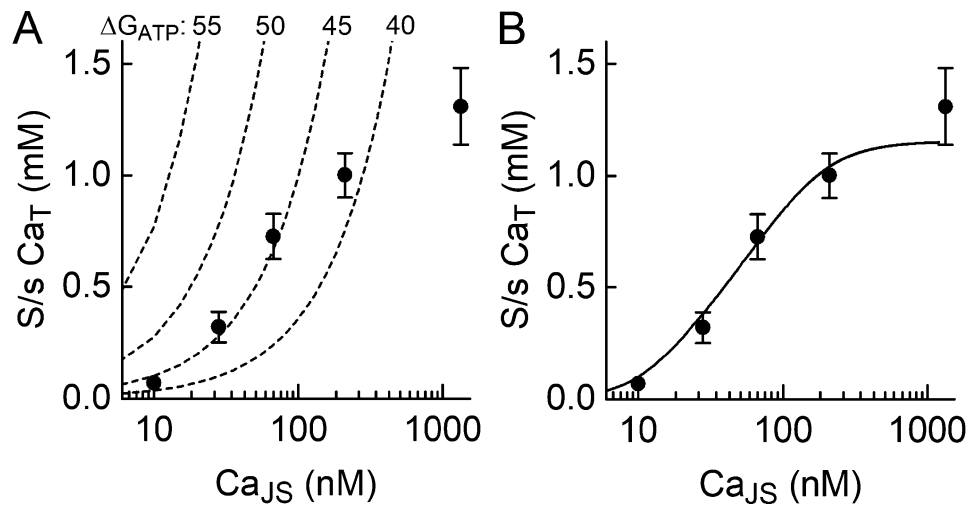


Figure 4. **Models to account for steady-state Ca<sub>T</sub>.** (A) Ca<sup>2+</sup> accumulation in the t-system limited by pump thermodynamics. The dashed curves show steady-state Ca<sub>T</sub>–Ca<sub>JS</sub> relationships for different  $\Delta G_{ATP}$  values. The curves show what steady-state Ca<sub>T</sub> would be if it was determined only by the ability of the pump to generate a gradient (Eq. 5). The symbols are experimental data (mean  $\pm$  SEM) determined in the presence of tetracaine; the independent variable for the experimental data was Ca<sub>M</sub>, but with RYRs blocked by tetracaine, Ca<sub>M</sub>  $\approx$  Ca<sub>JS</sub>, which drives the pump, both determined by the Ca<sup>2+</sup>–EGTA equilibrium. (B) Steady-state Ca<sub>T</sub> determined by balance between pumping Ca<sup>2+</sup> into the t-system and a concentration gradient-dependent leak of Ca<sup>2+</sup> out of t-system. The model used is given by Eqs. 6 and 7. Fitted parameters:  $c_{PMCA}$ , 60  $\mu\text{M}$ ;  $k_{Leak}^T$ , 0.023 s<sup>-1</sup>; and  $K_D^{PMCA}$ , 223  $\mu\text{M}$ .

appropriate comparison because in the absence of a Ca<sup>2+</sup> leak into the JS, Ca<sub>JS</sub>, which drives the pump, is determined by the Ca<sup>2+</sup>–EGTA equilibrium; thus, Ca<sub>JS</sub>  $\approx$  Ca<sub>M</sub> and can be estimated with some confidence.

To address the possibility that the thermodynamic limit of the pump determines steady-state Ca<sub>T</sub>, an expression was derived that relates maximum Ca<sub>T</sub> to Ca<sub>JS</sub> and  $\Delta G_{ATP}$ . As described by Smith et al. (2005), transport of Ca<sup>2+</sup> into the t-system, assuming that the Ca<sup>2+</sup>/ATP ratio is 2, occurs only when

$$\Delta G_{ATP} + 2\Delta G_{Ca} < 0, \quad (3)$$

where  $\Delta G_{Ca}$  depends on the ratio of Ca<sub>T</sub> to Ca<sub>JS</sub> and

$$\Delta G_{Ca} = RT \ln \left[ \frac{Ca_T}{Ca_{JS}} \right], \quad (4)$$

where  $R$  is the universal gas constant (8.314 J mol<sup>-1</sup> K<sup>-1</sup>) and  $T$  is the absolute temperature (298 K). Substituting Eq. 4 into Eq. 3 and rearranging to give an expression for the maximum Ca<sub>T</sub> that could be achieved by the pump if the thermodynamics were the only factor limiting Ca<sup>2+</sup> accumulation (hereafter called the limit Ca<sub>T</sub>):

$$\text{LimitCa}_T = Ca_{JS} \cdot e^{\frac{-\Delta G_{ATP}}{2 \cdot R \cdot T}}. \quad (5)$$

Eq. 5 was used to calculate the relationship between the limit Ca<sub>T</sub> and Ca<sub>JS</sub> for a series of values of  $\Delta G_{ATP}$ ; these are shown by the curves in Fig. 4 A. The range of  $\Delta G_{ATP}$  values used for the calculations (40–55 kJ mol<sup>-1</sup>) span the likely values in the skinned human muscle fibers. In intact skeletal muscle fibers,  $\Delta G_{ATP}$  is typically  $\sim$ 60 kJ mol<sup>-1</sup> (Barclay, 2015), but lower values are likely for skinned fibers, primarily owing to elevated inorganic phosphate concentration (Park-Holohan et al., 2010). The curves in Fig. 4 A can be used to estimate a lower limit for  $\Delta G_{ATP}$  in the skinned fibers. Even if PMCA thermodynamics did not

limit Ca<sup>2+</sup> accumulation, the pump must be capable of generating the observed Ca<sup>2+</sup> gradients. From Fig. 4 A, if  $\Delta G_{ATP}$  was 40 kJ mol<sup>-1</sup>, then the measured Ca<sub>T</sub> values for Ca<sub>JS</sub> of 28 and 67 nM were approximately fivefold higher than the pump could generate; therefore,  $\Delta G_{ATP}$  cannot have been that low. The curve for  $\Delta G_{ATP}$  of 45 kJ mol<sup>-1</sup> is close to the measured data points for Ca<sub>JS</sub> of 28 and 67 nM. This indicates that  $\Delta G_{ATP}$  in the fibers must have been  $\geq$ 45 kJ mol<sup>-1</sup>. However, the experimental Ca<sub>T</sub> values for Ca<sub>JS</sub> of 10, 210, and 1,340 nM lie substantially below the limit Ca<sub>T</sub>, so for those values, at least, some other mechanism must limit Ca<sup>2+</sup> accumulation in the t-system. In fact, the difference between the forms of the limit Ca<sub>T</sub>–Ca<sub>JS</sub> curves (increasing monotonically) and the experimental data (sigmoidal) precludes a thermodynamic pumping limit determining all the observed Ca<sub>T</sub> values.

The second idea is that there is passive leak of Ca<sup>2+</sup> out of the t-system, the rate of which depends on the [Ca<sup>2+</sup>] gradient between the t-tubule and the myoplasm. If it is assumed that the leak is a single process with a rate constant  $k_{Leak}^T$ , then when Ca<sub>T</sub> increases enough that the rate of leak,  $= k_{Leak}^T \times (Ca_T - Ca_{JS})$ , matches the rate of uptake of Ca<sup>2+</sup> into the system (determined by Ca<sub>JS</sub>), then Ca<sub>T</sub> will be constant. To see whether a scheme in which Ca<sup>2+</sup> pumping into the t-system is opposed by a leak can give a realistic Ca<sub>T</sub>–Ca<sub>JS</sub> relationship, a simple model was designed. For this proof-of-concept, it was assumed that (1) the rate of Ca<sup>2+</sup> pumping was described by the model developed by Tran et al. (2009) (Fig. 2 A); (2) the volume of the t-system was 20 times greater than the JS volume (Table 3); and (3) the Ca<sup>2+</sup> leaking out of the t-tubule did not alter the concentration of Ca<sup>2+</sup> driving the pump. These ideas are expressed in the differential equations

$$\frac{dCa_T}{dt} = \frac{1}{20} \cdot M_{PMCA}(Ca_J, Ca_T, K_D^{PMCA}, c_{PMCA}) - k_{Leak}^T \cdot Ca_T(t), \quad (6)$$

and

$$\frac{dCa_{JS}}{dt} = 0, \quad (7)$$

where  $M_{PMCA}$  is the rate of  $Ca^{2+}$  transfer between the JS and t-system by the PMCA, which is a function of  $[Ca^{2+}]$  on both sides of the t-tubule membrane, the pump's dissociation constant on the JS side of the membrane ( $K_D^{PMCA}$ ), and the concentration of the pump ( $c_{PMCA}$ ; for details, see Appendix 1).  $K_D^{PMCA}$ ,  $k_{Leak}^T$ , and  $c_{PMCA}$  were adjusted to give the least-squares fit between the model output and the experimental data. This model captures the characteristics of the observed data well (Fig. 4 B), matching the dependence of  $Ca_T$  on  $Ca_{JS}$  across the full  $Ca_{JS}$  range used in the experiments. In the remainder of the analysis, it was assumed that there was a  $Ca^{2+}$  leak from the t-tubule that, when a steady  $Ca_T$  was achieved, balanced the rate of uptake of  $Ca^{2+}$  into the t-system. Note, however, that PMCA model used ensures that, regardless of the other aspects of the overall model, the model pump will operate within its thermodynamic constraints.

To incorporate the t-system  $Ca^{2+}$  leak into the fiber model, it was important to decide the destination of the  $Ca^{2+}$  leaked from the t-system. The leaked  $Ca^{2+}$  could enter either the JS or the myoplasmic space. In trials, it was found that if the  $Ca^{2+}$  leaked into the JS then when  $Ca_M$  was  $<50$  nM, the leak caused a marked increase in  $Ca_{JS}$  and, consequently, predicted  $Ca_T$  values were higher than those observed. In contrast, when the leak was directed into the myoplasm, there was sufficient buffering to prevent changes in  $Ca_M$ , and the predicted  $Ca_T$  matched the observed  $Ca_T$ - $Ca_M$  relationship. Therefore, it was assumed that  $Ca^{2+}$  that leaked from the t-system entered the myoplasmic space.

**Estimating PMCA concentration.** If the rate at which  $Ca^{2+}$  accumulates in the t-system depends on the balance between the rates of  $Ca^{2+}$  uptake into and leak out of the t-system, then three parameters determine t-system  $Ca^{2+}$  accumulation:  $c_{PMCA}$ ,  $K_D^{PMCA}$ , and  $k_{Leak}^T$ . Values are not known for any of these parameters. Parameter optimization algorithms can be used to find a combination of values that will allow the model to match experimental data, but in this case such solutions are not unique because  $c_{PMCA}$  and  $k_{Leak}^T$  are not independent. Therefore, a value for one of the three parameters is required.

$c_{PMCA}$  could be estimated using Eq. 2, with the reported maximum rate of t-system  $Ca^{2+}$  accumulation (using Lagrange's notation,  $Ca_T'$ ). Cully et al. (2018) reported a mean maximum  $Ca_T'$  of  $170 \mu M s^{-1}$  (with the concentration referring to t-system volume). However, this rate is too high to be consistent with the overall time course of t-system  $Ca^{2+}$  accumulation. For example, when  $Ca_M$  is 67 nM and tetracaine is present,  $Ca_T$  increases with a half-time ( $t_{1/2}$ ) between 15 and 20 s, and  $>60$  s is required to reach a final steady  $Ca_T$  (e.g., Fig. 5 A). If the maximum rate of  $Ca^{2+}$  pumping is  $170 \mu M s^{-1}$ , then by Eq. 2,  $c_{PMCA}$  would be  $280 \mu M$ , with concentration expressed relative to JS volume. Using that concentration, the model predicts that  $Ca_T$  will reach a steady value in  $\sim 15$  s, regardless of the value of  $k_{Leak}^T$ . This suggests that the reported maximum  $Ca_T'$  is not representative of the overall uptake of  $Ca^{2+}$  into the t-system.

As an alternative, a modeling-based method was used to estimate  $c_{PMCA}$ . The simple PMCA/leak model described above (Eqs. 6 and 7) was used to find combinations of  $c_{PMCA}$  and  $k_{Leak}^T$  that produce records of t-system  $Ca^{2+}$  accumulation consistent with the observed rate of increase in  $Ca_T$  and its final magnitude. Using the best-fit parameters from the preliminary analysis of the pump/leak model (Fig. 4 B) as a starting point, a detailed Monte Carlo analysis was performed in which the time course of increase in  $Ca_T$  was calculated using the model for 5,000 combinations of  $c_{PMCA}$  and  $k_{Leak}^T$ , each selected at random from a range of  $\pm 50\%$  of the preliminary values (Fig. 5 B). The criteria set for a record to be considered consistent with observed data were that  $t_{1/2}$  was between 15 and 20 s and the maximum  $Ca_T$  was between 690 and 770  $\mu M$  ( $\pm 5\%$  of the reported mean value; Cully et al., 2018). Records meeting the criteria were identified (i.e., those that passed through the red rectangle and finished between the horizontal red lines in Fig. 5 B), and the combinations of  $c_{PMCA}$  and  $k_{Leak}^T$  giving rise to such records were plotted (Fig. 5 C). To determine the effect of the third influential parameter,  $K_D^{PMCA}$ , the analysis was performed for three values of  $K_D^{PMCA}$  that span the range of likely values;  $K_D^{PMCA}$  is constrained by the range of  $[Ca^{2+}]$  corresponding to the sloping section of the  $Ca_T$ - $Ca_M$  relationship (Fig. 4 B). The results of this analysis are shown in Fig. 5 C.

For each value of  $K_D^{PMCA}$ ,  $\sim 200$  records were identified as being consistent with the observed time course and magnitude of t-system  $Ca^{2+}$  accumulation; the combinations of  $c_{PMCA}$  and  $k_{Leak}^T$  that gave those records are plotted in Fig. 5 C. For each value of  $K_D^{PMCA}$ , the range of pump concentrations that can give a time course consistent with those observed is  $\sim 15 \mu M$ . As a best estimate of  $c_{PMCA}$ , the value in the middle of the complete range was taken; this was  $58 \mu M$ . This value, with selection of an appropriate  $k_{Leak}^T$ , is able to accurately simulate the  $Ca_T$  time course across the full range of  $K_D^{PMCA}$  values tested.  $c_{PMCA}$  is expressed relative to the JS volume (Table 3), which is appropriate because the rate of  $Ca^{2+}$  pumping is set by  $Ca_{JS}$  and the  $c_{PMCA}$  in that volume. Note that although  $c_{PMCA}$  is numerically similar to  $c_{SERCA}$ , when the difference in volume between the JS and myoplasm (Table 3), and in the surface area of the t-system and SR (Eisenberg, 1983), are taken into account, the current analysis suggests that the density of  $Ca^{2+}$  pumps in the t-system membrane is  $<1\%$  of that for the SR membrane.

In Fig. 5 D, a comparison is shown of the measured record of the time course of  $Ca_T$  from Fig. 5 A and that calculated using the PMCA/leak model with  $c_{PMCA}$  of  $58 \mu M$ ,  $k_{Leak}^T$  of  $0.02 s^{-1}$ , and  $K_D^{PMCA}$  of  $200 \mu M$  (corresponding to pump  $Ca_{50} = 40$  nM). The time courses match well, although the model indicates that the experimental protocol did not allow sufficient time for  $Ca_T$  to reach a complete plateau. Overall, the analysis presented in this section shows that a model of t-system  $Ca^{2+}$  accumulation consisting of PMCA, driven by a constant  $[Ca^{2+}]$ , and a concentration gradient-dependent  $Ca^{2+}$  leak from the t-system can accurately describe both the steady-state  $Ca_T$ - $Ca_M$  relationship measured in the presence of tetracaine (Fig. 4 B) and the time course with which  $Ca^{2+}$  accumulates in the t-system (Fig. 5 D).

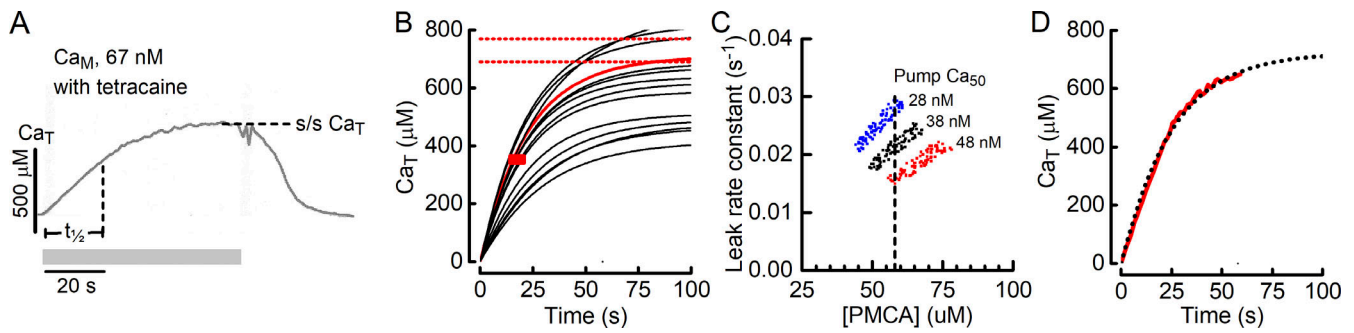


Figure 5. **Estimating the concentration of PMCA in the JS.** (A) An example of the time course of  $Ca^{2+}$  accumulation in the t-system. The t-system was initially depleted of  $Ca^{2+}$ , and  $Ca^{2+}$  ( $Ca_M$ , 67 nM) was returned to the fiber for the period indicated by the gray bar. Tetracaine was included in the bathing solution to inhibit RYR  $Ca^{2+}$  leak. In that case,  $Ca_{JS}$ , which drives PMCA, can be considered to equal  $Ca_M$ . Steady-state  $Ca_T$ , steady-state  $[Ca^{2+}]$ ;  $t_{1/2}$ , time to reach 50% of steady-state  $Ca_T$ . (B) Model-generated time courses of  $Ca^{2+}$  accumulation in the t-system using different combinations of PMCA concentration and  $k_{Leak}^T$ . The example shows 15 records; the complete analysis used 5,000 records. Parameter combinations that produced records with realistic values of  $t_{1/2}$  and steady-state  $Ca_T$  were those that passed through the red rectangle (correct  $t_{1/2}$ ) and reached a final  $Ca_T$  value between the horizontal red lines. The one record in the sample meeting these criteria is shown in red. (C) Combinations of  $c_{PMCA}$  and  $k_{Leak}^T$  that are consistent with observed time course of t-system filling. The analysis was performed for three  $K_D^{PMCA}$  values (150, 200, and 250  $\mu M$ ) that span the range of likely values; these correspond to pump  $Ca_{50}$  values of 28, 38, and 48 nM under the conditions in the skinned fibers. Vertical dashed line, the value chosen for  $c_{PMCA}$  that can fulfill the requirement of producing realistic time course of t-system  $Ca^{2+}$  accumulation across the range of likely  $K_D^{PMCA}$  values. (D) Comparison of measured (solid red line) and calculated (dotted black line) time courses of  $Ca^{2+}$  accumulation in the t-system. The measured record is a digitized version of the record in A, and the calculated record was generated using the fiber model with parameter values:  $c_{PMCA}$ , 58  $\mu M$ ;  $k_{Leak}^T$ , 0.018  $s^{-1}$ ; and  $K_D^{PMCA}$ , 210  $\mu M$  ( $Ca_{50}$ , 40 nM).

### Buffering of $Ca^{2+}$ by EGTA in JS and myoplasm

$Ca^{2+}$  was buffered by exogenous EGTA (50 mM) in the myoplasm and JS. Binding of  $Ca^{2+}$  by EGTA was assumed to be a second-order reaction (Eq. 8) with a dissociation constant of 0.18  $\mu M$  under the conditions used for the experiments and an off-rate of 0.3  $s^{-1}$  (Smith et al., 1984). The on-rate constant was then 0.3  $s^{-1}/0.18 \mu M = 1.67 \mu M^{-1} s^{-1}$ . The variations of bound and free  $Ca^{2+}$  with total  $[Ca^{2+}]$  are shown in Fig. 5 A.

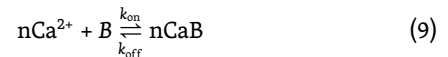


### Buffering of $Ca^{2+}$ in the SR

In resting muscle fibers, most of the  $Ca^{2+}$  is in the SR, and most of that is bound to Csq and, probably, to other unidentified buffers (Manno et al., 2013). The buffering of  $Ca^{2+}$  in the SR is an important component of the model, as it was assumed that the rate of  $Ca^{2+}$  leak through the RYRs depended on the  $Ca^{2+}$  concentration gradient between the SR and JS. In the protocols used in the fiber experiments,  $Ca_{JS}$  was maintained in the submicromolar range by its equilibrium with EGTA; in that case, the rate of leak is primarily determined by  $Ca_{SR}$  (typically 400–1,000  $\mu M$ ) and is thus influenced by the features of  $Ca^{2+}$  buffering in the SR. Additionally, the protocol for measuring RYR  $Ca^{2+}$  leak starts with the SR depleted of  $Ca^{2+}$ ; therefore, the magnitude of the leak will, at least initially, be time dependent, reflecting the time course with which  $Ca_{SR}$  increases, and so is likely to be influenced by  $Ca^{2+}$ -buffering kinetics.

The mechanism of  $Ca^{2+}$  buffering in the SR is not understood, but the buffering profile has been mapped by Manno et al. (2013), and this was used as a benchmark for the model. Following Lee and Keener (2008), the SR  $Ca^{2+}$  buffer molecules (B) were assumed to have an average of  $n$  binding

sites, all of which are either simultaneously occupied by  $Ca^{2+}$  or simultaneously empty; this scheme provides the cooperative binding apparent in the observed  $Ca^{2+}$  buffering in the SR (Pape et al., 2007; Manno et al., 2013). The reaction scheme and the associated differential equation are



and

$$\frac{dCaB}{dt} = k_{on} \cdot Ca_{SR}(t)^n \cdot (B_{Tot} - CaB) - k_{off} \cdot CaB. \quad (10)$$

In Eq. 9, B is buffer, CaB is  $Ca^{2+}$  bound to the buffer molecule, and  $k_{on}$  and  $k_{off}$  are the rate constants for association and dissociation, respectively. In Eq. 10,  $B_{Tot}$  is the total concentration of buffer sites,  $CaB$  is the concentration of buffer sites with  $Ca^{2+}$  bound,  $B_{Tot} - CaB$  is the concentration of available buffer sites, and  $n$  is the cooperativity coefficient. Manno et al. (2013) estimated that the concentration of  $Ca^{2+}$  buffer sites was  $\sim 70$  mM (with respect to SR volume), and this value was used in the model. The rate constants are related to the dissociation constant by  $K_D^B = (k_{off}/k_{on})^{1/n}$ . Dissociation of the  $Ca^{2+}$ -buffer complex is rapid (Baylor and Hollingworth, 2003; Sztrye et al., 2011a), so  $k_{off}$  was set to 3,000  $s^{-1}$ . The SR  $Ca^{2+}$  buffering properties of mouse muscle are well described by a sigmoidal relationship, with  $K_D^B = 460 \mu M$  and  $n = 3.5$  (Manno et al., 2013). With only a slight adjustment to  $K_D^B$  (450  $\mu M$ ), using these values in the current model (solid line, Fig. 6 B) provided a close match to the empirical SR  $Ca^{2+}$  buffering curve described by Manno et al. (2013) (Fig. 6 B, black line). Using these values,  $k_{on} = k_{off}/e^{n \cdot \ln(K_D^B)} = 3,000/e^{3.5 \cdot \ln(450)} = 1.55 \times 10^{-6} \mu M^{-1} s^{-1}$ . Fig. 6 C shows the variation in bound and unbound  $[Ca^{2+}]$  as a function of total SR content. A notable feature is that when the SR  $Ca^{2+}$  content is low, the  $Ca^{2+}$  buffering power is low. Consequently, during the



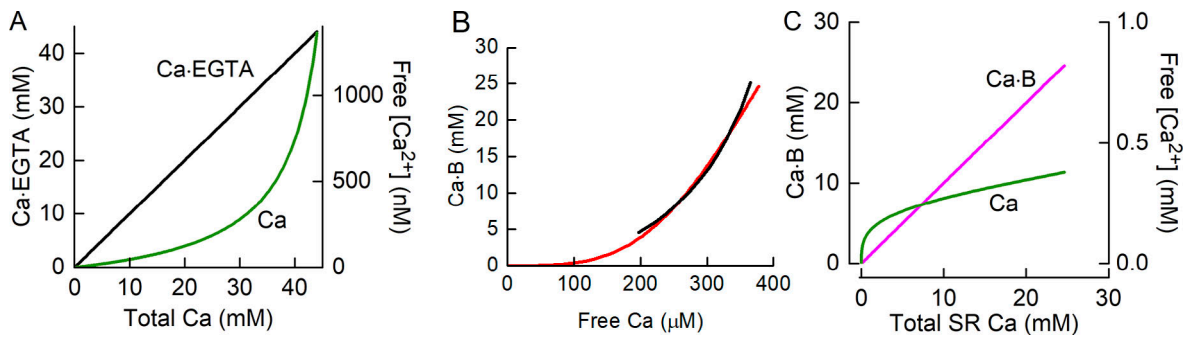


Figure 6. **Characteristics of  $\text{Ca}^{2+}$  buffers.** (A)  $\text{Ca}^{2+}$ -EGTA dissociation curve. Variation of concentrations of bound  $\text{Ca}^{2+}$  (Ca-EGTA; black line, left y axis) and unbound or free  $\text{Ca}^{2+}$  (Ca; green line, right y axis) with total  $\text{Ca}^{2+}$ . Note the  $10^6$ -fold difference in the scales of the y axes. (B) Equilibrium binding curve for SR  $\text{Ca}^{2+}$  buffers (including Csq). Solid red curve, relationship for the model used in the current study determined from equilibrium solution of Eq. 10 with total buffer  $\text{Ca}^{2+}$  binding site concentration = 70 mM,  $K_D^B = 450 \mu\text{M}$ , and  $n = 3.5$ . Black curve, the empirical relationship determined by Manno et al. (2013; from their Fig. 7 A). (C) SR- $\text{Ca}^{2+}$  buffer dissociation curve showing variations in bound  $\text{Ca}^{2+}$  (Ca-B; magenta line, left x axis) and unbound, or free,  $\text{Ca}^{2+}$  (green line, right x axis) with total SR  $\text{Ca}^{2+}$  content.

initial stages of SR filling (after prior  $\text{Ca}^{2+}$  depletion),  $\text{Ca}_{\text{SR}}$  will increase with little increase in  $\text{Ca}_B$ .

#### Buffering of $\text{Ca}^{2+}$ by TnC in the myoplasm

TnC binds  $\text{Ca}^{2+}$  in its role of linking the contractile response to the release of  $\text{Ca}^{2+}$  into the myoplasm. Fast-twitch mammalian muscle myoplasm contains  $\sim 200 \mu\text{M}$  of TnC  $\text{Ca}^{2+}$  binding sites, and at rest,  $\sim 30\%$  of the sites have  $\text{Ca}^{2+}$  bound. The question of relevance to the current model is, can TnC can bind sufficient  $\text{Ca}^{2+}$  so that the free  $\text{Ca}^{2+}$  is not simply that expected from the total  $\text{Ca}^{2+}$  in the fiber and the kinetics of  $\text{Ca}^{2+}$  binding by EGTA? To address this question, a model was developed of  $\text{Ca}^{2+}$  binding by TnC and EGTA. The model is described in detail in Appendix 2. The modeling illustrated that  $\text{Ca}^{2+}$  binding by TnC would have a negligible effect on the free  $\text{Ca}^{2+}$  calculated from just the  $\text{Ca}^{2+}$ -EGTA reaction. For example, when the free  $\text{Ca}^{2+}$  is intended to be  $1 \mu\text{M}$ , the presence of TnC would reduce the actual free  $[\text{Ca}^{2+}]$  by 0.1%; the effect is even smaller for lower free  $[\text{Ca}^{2+}]$ . Consequently, it was not necessary to include  $\text{Ca}^{2+}$  binding by TnC in the model.

#### Diffusive exchange of $\text{Ca}^{2+}$ between JS and myoplasm

In the absence of a leak of  $\text{Ca}^{2+}$  into the JS, there is little difference between  $\text{Ca}_{\text{JS}}$  and  $\text{Ca}_M$  because both are controlled by the equilibrium with EGTA. In the presence of a leak, it would be expected that  $\text{Ca}_{\text{JS}}$  increases as  $\text{Ca}^{2+}$  is added to the JS, despite the buffering by EGTA. The observation that a steady, sub-maximal  $\text{Ca}_T$  is achieved when  $\text{Ca}_M$  is at levels too low to achieve maximal pumping by PMCA indicates that there is a mechanism that limits the increase in  $\text{Ca}_{\text{JS}}$ . We assumed that this was diffusion of  $\text{Ca}^{2+}$  between the JS and myoplasm. The diffusion rate was adjusted so that the model steady-state  $\text{Ca}_T$  matched the experimentally determined values. That is, in the steady state, the sum of the leak of  $\text{Ca}^{2+}$  from the t-system into the myoplasm and the diffusive movement from the JS to the myoplasm equaled the rate at which  $\text{Ca}^{2+}$  was added to the JS via the RYRs. The diffusive exchange was

modeled as a simple movement of  $\text{Ca}^{2+}$  depending on the difference ( $\text{Ca}_{\text{JS}} - \text{Ca}_M$ ).

#### Relative volumes of physical compartments

The physiologically relevant  $\text{Ca}^{2+}$  concentrations (e.g., for stimulating pumps or driving diffusive exchanges) are those expressed with respect to the volume of water within individual compartments rather than to fiber water volume. Therefore, the relative volumes of the different compartments were taken into account when determining the concentration changes resulting from exchanges between compartments. For example, in human vastus lateralis muscle, the relative volume of the SR is  $\sim 100$  times that of the JS (Eisenberg, 1983), so that movement of  $\text{Ca}^{2+}$  from the SR to the JS results in an increase in  $[\text{Ca}^{2+}]_{\text{JS}}$  that is 100-fold greater than the corresponding decrease in  $[\text{Ca}^{2+}]_{\text{SR}}$ . The proportions of fiber volume accounted for by each physical compartment are shown in Table 3.

The JS is a conceptual rather than physical space, and its volume is difficult to both define and estimate; it is a region between the RYRs and the adjacent t-tubule. We estimated  $V_{\text{JS}}$ , relative to that of the t-tubule ( $V_{\text{TT}}$ ), on the basis that (1) t-tubule diameter is 85 nm (Jayasinghe and Launikonis, 2013), (2) the distance between the SR and t-tubules is 12 nm (Mitchell et al., 1983; Franzini-Armstrong et al., 1999), (3) the RYRs are 30 nm in diameter and the spacing between the centers of closest adjacent units is 100 nm (Franzini-Armstrong et al., 1999), and (4) the RYRs are arranged in a double layer, with one layer on either side of the t-tubule (Jayasinghe et al., 2014). The volume of a space with the same diameter as the RYR and the t-tubule was calculated, and it corresponded to  $\sim 4\% V_{\text{TT}}$  if the t-tubule cross-section is circular and 5% if elliptical (Jayasinghe and Launikonis, 2013), with the major axis length twice that of the minor axis. This range of values is consistent with the 4.5% calculated by Dulhunty et al. (1992). In the simulations,  $V_{\text{JS}}$  was set to  $5\% V_{\text{TT}}$ .

Unless otherwise specified, concentrations are expressed relative to the compartment in which the relevant molecular

species is contained. For example, concentrations in the myoplasm are expressed with respect to myoplasmic water volume. The data used to calculate myoplasmic water volume and the concentration conversion values are presented in [Table 3](#).

### Composition of myoplasmic and JSs

The rates of  $\text{Ca}^{2+}$  movement by SERCA and PMCA depend on the concentrations of ATP and its metabolites and on pH. These values are largely determined by the composition of the solutions used with the skinned fiber preparation ([Cully et al., 2018](#)). Assumed concentrations (in mM) were as follows: myoplasm/JS: 8 ATP, 0.05 ADP, and 1 Pi; t-tubule:  $\text{Ca}^{2+}$ , time dependent and calculated using the model. pH in all spaces was taken to be 7.1. The rate of  $\text{Ca}^{2+}$  pumping by SERCA and PMCA is strongly influenced by ADP concentration and pH ([Inesi and Hill, 1983](#); [Tran et al., 2009](#)). It was assumed that [ADP] and pH were constant during an experiment, with pH buffered by HEPES in the bathing solution and ATP, and hence ADP, buffered by endogenous creatine kinase, presumably bound to intracellular structures ([Dzeja and Terzic, 2003](#)).

### Experimental data

The experimental data used in this study are those referred to in [Cully et al. \(2018\)](#) that describe the uptake of  $\text{Ca}^{2+}$  into the t-system of fibers from human vastus lateralis muscle. The data are from the control group in that study and as such had no apparent abnormalities in  $\text{Ca}^{2+}$  handling. Briefly, the experimental protocol involved first depleting the SR and t-system of  $\text{Ca}^{2+}$  by exposing the fibers to caffeine, which kept the RYRs and store-operated  $\text{Ca}^{2+}$  channels on the t-system open. The caffeine was removed, and the fibers were placed in a solution with a known  $\text{Ca}^{2+}$  concentration. The time course with which  $\text{Ca}^{2+}$  entered the t-system was monitored using the  $\text{Ca}^{2+}$ -sensitive compound rhod-5N trapped inside the t-tubules.

### Implementing the model

The modeling was carried out using Maple (v2016.1) and MapleSim (v2016) software (Maplesoft). The model equations were deployed, and parameter values were entered in the general mathematics environment provided by Maple. The system of differential equations was solved numerically using the Rosenbrock method ([Rosenbrock, 1963](#)). To be consistent with the experimental protocol ([Cully et al., 2018](#)), simulations commenced with the SR and T systems depleted of  $\text{Ca}^{2+}$  so that all the  $\text{Ca}^{2+}$  was in the myoplasm and JS and in equilibrium with EGTA. The total  $\text{Ca}^{2+}$  was set to give the desired myoplasmic free  $[\text{Ca}^{2+}]$ , as determined by the EGTA- $\text{Ca}^{2+}$  equilibrium ([Fig. 6 A](#)). The differential equations are shown in Appendix 1. Once the model was developed, the equations were imported into MapleSim to create a fast, compiled version of the model, which was used for subsequent analysis using Maple. Using a computer with a 2.2-GHz processor and 8 GB of memory, the compiled version simulated 120 s of t-system  $\text{Ca}^{2+}$  accumulation in 8 ms.

To quantify the rate of  $\text{Ca}^{2+}$  leak from RYRs,  $c_{\text{PMCA}}$  was fixed at 58  $\mu\text{M}$ , and  $K_{\text{D}}^{\text{PMCA}}$  and  $k_{\text{Leak}}^{\text{T}}$  were treated as variables whose values were those that provided the least-squares fit of the model to the empirical  $\text{Ca}_{\text{T}}-\text{Ca}_{\text{M}}$  relationship determined in the

presence of tetracaine (see Results). This was done by creating a function that returned the model-calculated maximum  $\text{Ca}_{\text{T}}$  for specified values of  $\text{Ca}_{\text{M}}$ ,  $K_{\text{D}}^{\text{PMCA}}$ , and  $k_{\text{Leak}}^{\text{T}}$  and using that function in a nonlinear regression fitting routine implemented using Maple software.

## Results

### Identifying parameters that influence t-system $\text{Ca}^{2+}$ accumulation

Parameters that influenced t-system  $\text{Ca}^{2+}$  accumulation were identified using a Monte Carlo analysis in which the model was solved for many random combinations of parameter values. The analysis was performed using nine parameters selected on the basis that their location in the model might allow them to influence t-system  $\text{Ca}^{2+}$  accumulation. The results of the analysis are summarized in [Table 4](#) and [Fig. 7](#). In [Fig. 7](#), influences of four parameters are illustrated graphically: the cloud of light gray symbols are the  $\text{Ca}_{\text{T}}$  ([Fig. 7, A-D](#)) and  $t_{1/2}$  ([Fig. 7, E-H](#)) values calculated from 4,000  $\text{Ca}_{\text{T}}$  versus time curves with random combinations of the nine parameters, and the solid lines show the variation in  $\text{Ca}_{\text{T}}$  or  $t_{1/2}$  as a function of only the parameter of interest. To quantify the influence of each parameter, the square of the correlation coefficient ( $r^2$ ) was calculated from the least-squares fit of a second-order polynomial through the data cloud, with the parameter of interest as the independent variable.  $r^2$  is the fraction of the total variance, arising from all the parameters assessed, that can be attributed to the parameter of interest. The  $r^2$  values for all the parameters assessed are shown in [Table 4](#), which includes analyses for  $\text{Ca}_{\text{M}}$  of both 67 and 1,340 nM.

The four parameters with the greatest influence on  $\text{Ca}^{2+}$  accumulation in the t-system were those directly involved in the t-system—PMCA concentration and  $\text{Ca}^{2+}$  sensitivity (quantified by  $K_{\text{D}}^{\text{PMCA}}$ ) and the magnitude of the  $\text{Ca}^{2+}$  leak from the t-system—and the  $\text{Ca}^{2+}$  leak through the RYRs. These parameters accounted for ~75% of the total variance in steady-state  $\text{Ca}_{\text{T}}$  and  $t_{1/2}$ . The extent of t-system filling was mainly determined by  $c_{\text{PMCA}}$  ([Fig. 7 A](#)) and t-system leak rate ([Fig. 7 C](#)); this is consistent with the notion that the level of filling reflects the balance between rate of  $\text{Ca}^{2+}$  uptake into the t-system, which depends on  $c_{\text{PMCA}}$ , and the leak of  $\text{Ca}^{2+}$  from the t-system. The size of the RYR leak rate constant also influences the magnitude of  $\text{Ca}_{\text{T}}$ , which is desirable given that the purpose of the protocol was to use changes in  $\text{Ca}_{\text{T}}$  to estimate RYR leak. It should be noted, however, that although  $k_{\text{Leak}}^{\text{RyR}}$  influenced the extent of  $\text{Ca}^{2+}$  accumulation when  $\text{Ca}_{\text{M}}$  is lower than that required to fully activate PMCA (e.g., 67 nM), it had no influence when  $\text{Ca}_{\text{M}}$  is high (1,340 nM). In the latter case, the pump is operating maximally even in the absence of RYR leak, so any further addition of  $\text{Ca}^{2+}$  to the JS by the leak would not affect the rate at which  $\text{Ca}^{2+}$  is pumped into the t-system.

It is apparent from [Table 4](#) that parameters associated with the SR  $\text{Ca}^{2+}$  pump (the right three columns of [Table 4](#)) had little influence on  $\text{Ca}^{2+}$  accumulation in the t-system. This indicates that the time course of increase in  $\text{Ca}_{\text{SR}}$ , and any effect that has on RYR  $\text{Ca}^{2+}$  leak and thus  $\text{Ca}_{\text{JS}}$ , does not limit the pumping of  $\text{Ca}^{2+}$  from the JS into the t-system.

Table 4.  $r^2$  values for dependence of steady-state  $Ca_T$  and  $t_{1/2}$  on selected model parameters

$Ca_M$	$c_{PMCA}$	$k_{Leak}^T$	$K_D^{PMCA}$	$V_{JS}$	$k_{Leak}^{RyR}$	$k_{Diff}$	$K_D^{SERCA}$	$c_{SERCA}$	$k_{Leak}^{SR}$
<b>67</b>									
Max. $Ca_T$	0.3	0.2	0.19	0.15	0.12	0.03	0.015	0.002	0.001
$t_{1/2}$	0.2	0.38	<0.001	0.34	0.01	0.04	0.007	<0.001	0.001
<b>1,340</b>									
Max. $Ca_T$	0.41	0.2	0.001	0.41	<0.001	0.001	<0.006	<0.003	<0.001
$t_{1/2}$	0.184	0.62	<0.001	0.19	<0.001	<0.001	<0.001	<0.001	<0.001

### Steady-state $Ca_T$ - $Ca_M$ relationship

Uptake of  $Ca^{2+}$  into the t-system has been characterized by the relationship between the ultimate extent of  $Ca^{2+}$  accumulation and the concentration of  $Ca^{2+}$  in the myoplasmic solution (i.e., the  $Ca_T$ - $Ca_M$  relationship; Fig. 4 B). From Fig. 7, it is apparent that steady-state  $Ca_T$  depends on  $c_{PMCA}$ ,  $K_D^{PMCA}$ , and the rate constants for the  $Ca^{2+}$  leaks from the t-system and through the RYRs. The value of  $c_{PMCA}$  was fixed (see Materials and methods) but the values of  $K_D^{PMCA}$ ,  $k_{Leak}^T$ , and  $k_{Leak}^{RyR}$  are not known. Those values were determined using the model by finding the parameter values that gave the least-squares fit of the model to the experimental  $Ca_T$ - $Ca_M$  data. There were two steps to this

analysis. First,  $K_D^{PMCA}$  and  $k_{Leak}^T$  were determined using data obtained in the presence of tetracaine, because in that case it was assumed there was no RYR  $Ca^{2+}$  flux, so  $k_{Leak}^{RyR} = 0$ . It was then assumed that  $K_D^{PMCA}$  was unaffected by tetracaine but that, as preliminary analysis revealed,  $k_{Leak}^T$  did depend on whether the RYRs were functional. Therefore, the second part of the analysis was to use data obtained without tetracaine to determine  $k_{Leak}^T$  (in the absence of tetracaine) and  $k_{Leak}^{RyR}$ . The results of the fitting procedure are shown in Fig. 8 A, and the parameter values are given in Table 5.

The shape of the  $Ca_T$ - $Ca_M$  relationship predicted by the model matches the experimental data well (Fig. 8 A), indicating

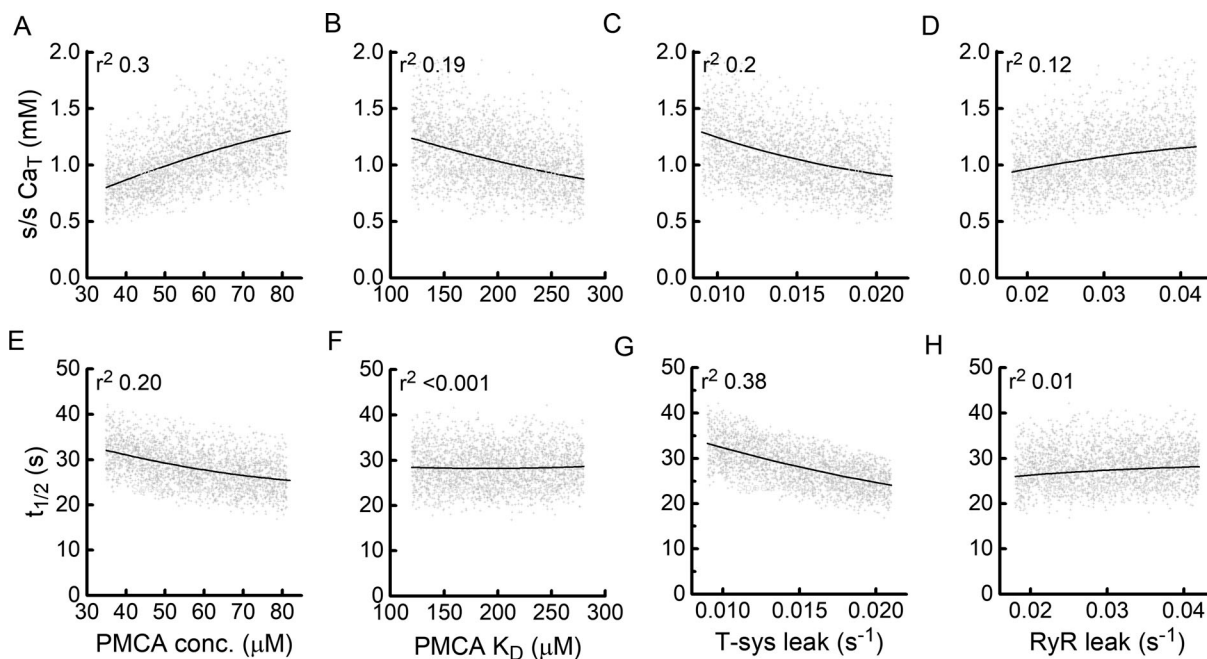


Figure 7. **Sensitivity of t-system  $Ca^{2+}$  accumulation to most influential parameters.** (A–H) Each graph shows the variation with one parameter of steady-state  $Ca_T$  (A–D) and rate of accumulation of  $Ca^{2+}$  in the t-system as quantified by the time taken for  $Ca_T$  to reach 50% of its final value ( $t_{1/2}$ , E–H). Gray points are individual values determined using a Monte Carlo analysis (i.e., 4,000 random combinations of nine parameters). The solid lines are values calculated, using the model, for variation in just the parameter of interest with all other parameter values held constant. The analyses were performed for a  $Ca_M$  of 67 nM; the random parameter values were chosen from a range of values spanning  $\pm 40\%$  around typical values. A larger span ( $\pm 60\%$ ) was used for RYR leak rate constant. The vertical scatter of the data points reflects the variance from the influences of all the parameters included in the analysis, and the vertical displacement of the solid lines reflects the variance attributable to that parameter. The  $r^2$  value quantifies the ratio of these two variances.

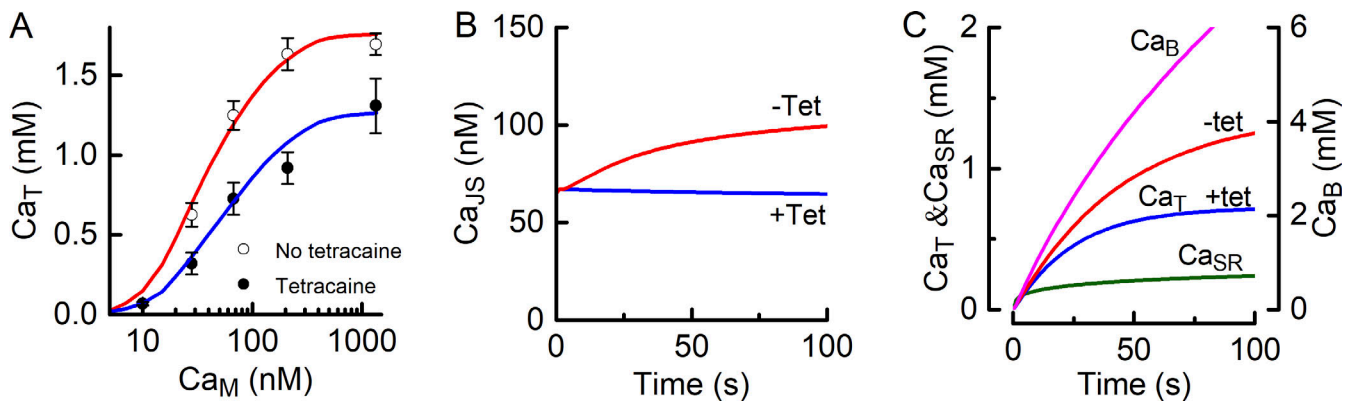


Figure 8. **Model predictions.** (A) Comparison of experimental data and model. Symbols represent mean ( $\pm$  SEM)  $Ca_T$  data with (filled circles) and without (open circles) tetracaine. The curves are the best fits of the model to the data points. For the tetracaine case (blue line), the model was fitted by adjusting the values of the t-system  $Ca^{2+}$  leak and  $K_D^{PMCA}$ . For the non-tetracaine case (red line),  $K_D^{PMCA}$  was assumed to be the same as in the presence of tetracaine, and the parameters adjusted to obtain the best fit were the rate constants for the t-system leak and RYR leak. The parameter values are given in Table 5. (B) Model-derived time courses of  $Ca_{JS}$  in the presence (+Tet, blue line) and absence (-Tet, red line) of a leak of  $Ca^{2+}$  through the RYRs. When there is no RYR  $Ca^{2+}$  leak,  $Ca_{JS}$  is maintained by the equilibrium with EGTA and diffusion of  $Ca^{2+}$  from the myoplasm. In the presence of a RYR  $Ca^{2+}$  leak into the JS (red line), sufficient  $Ca^{2+}$  enters the JS to increase the unbound  $[Ca^{2+}]$ . (C) Model-derived time courses of  $[Ca^{2+}]$  in the SR and t-system in the presence of RYR  $Ca^{2+}$  leak. Most  $Ca^{2+}$  entering the SR binds to SR  $Ca^{2+}$  buffers ( $Ca_B$ , right-hand y scale).

that the model included sufficient detail to describe t-system  $Ca^{2+}$  accumulation in the experimental preparation. In the absence of RYR  $Ca^{2+}$  leak, the calculated  $K_D^{PMCA}$  and  $k_{Leak}^T$  values (Table 5) give rise to a  $Ca_T$ - $Ca_M$  relationship with a  $Ca_{50}^{PMCA}$  of  $\sim 67$  nM. Withdrawal of tetracaine had two clear effects. (1) The leak of  $Ca^{2+}$  from the t-system was reduced, which increased steady-state  $Ca_T$  values.  $k_{Leak}^T$  in the absence of tetracaine was 60% of that in the presence of tetracaine. (2)  $Ca^{2+}$  leak through the RYRs was apparent ( $k_{Leak}^{RyR} = 0.035$  s $^{-1}$ ), which shifted the  $Ca_T$ - $Ca_M$  curve to the left of that determined with tetracaine;  $Ca_{50}^{PMCA}$  was reduced to 42 nM. It is difficult to distinguish these two effects—increased RYR leak and decreased t-system leak—by inspection, but they were readily revealed and quantified using the model curve-fitting procedure.

The rate constants for the two  $Ca^{2+}$  leaks (Table 5) were combined with known values for  $Ca_{SR}$  and  $Ca_T$  to calculate the rates of  $Ca^{2+}$  exchanges among fiber compartments. These calculations were done using steady-state data corresponding to  $Ca_M$  of 67 nM, this being approximately the free  $[Ca^{2+}]$  in unstimulated, intact muscle fibers, and assuming that RYR leak was as determined in the skinned fiber preparation in the absence of tetracaine. The steady-state movements of  $Ca^{2+}$  in the

skinned fiber preparation are summarized in Fig. 9. The flows were calculated using concentrations of  $Ca^{2+}$  in the SR and t-system and the rate constants for leaks from those compartments (Table 5). For example, the rate of  $Ca^{2+}$  leak from the t-system can be calculated:  $k_{Leak}^T \times \text{steady-state } Ca_T = 0.013$  s $^{-1} \times 1,200$   $\mu$ M = 15.6  $\mu$ M s $^{-1}$ , and this is the same as the rate of uptake of  $Ca^{2+}$  into the t-system by PMCA in the steady state. This sets the rate at which  $Ca^{2+}$  is removed from the JS, and so on. In Fig. 9, the flows are quantified according to the volumes of both the origin and destination compartments (Table 3). For example, an outflow (indicated by -) of 14  $\mu$ M s $^{-1}$  from the SR produces an influx (+) into the JS, in terms of JS volume, of  $14 \times (3.8 / 0.014) = 3,800$   $\mu$ M s $^{-1}$ . Note that in a steady state, the amount of  $Ca^{2+}$  bound to EGTA will be constant and thus does not need to be considered in this analysis.

A notable feature of the  $Ca^{2+}$  flows is that only a small fraction of the  $Ca^{2+}$  calculated to leak into the JS is pumped into the t-system: of the influx of 3,800  $\mu$ M s $^{-1}$ , 312  $\mu$ M s $^{-1}$ , or 8%, is pumped into the t-system, and the remainder must diffuse into the myoplasmic space. This is, at least in part, a consequence of the low density of PMCA in the JS, as calculated in Materials and methods. A second notable aspect is that  $\sim 20\%$  of the  $Ca^{2+}$  pumped into the SR leaks into the JS, and the remainder leaks into the myoplasm. Therefore, under resting conditions in the skinned fiber, most of the cycling  $Ca^{2+}$  leaked from the SR into the myoplasm, presumably via a SERCA-related mechanism; one-fifth leaked into the JS via RYRs; and only a small fraction of that passed through the PMCA.

#### Time course of $Ca^{2+}$ movements during t-system $Ca^{2+}$ accumulation

The model provides a means of estimating the time course of  $Ca^{2+}$  movements during the protocol used to determine  $Ca^{2+}$  t-system accumulation. In Fig. 8 B, the time courses of  $Ca^{2+}$  concentration in the myoplasm and JS are shown for a RYR leak

Table 5. **Parameter values determined from fitting model to  $Ca_T$  versus  $Ca_M$  data**

Parameter	With tetracaine	Without tetracaine
$k_{Leak}^T$ (s $^{-1}$ )	0.022 (0.017–0.030)	0.013 (0.009–0.016)
$K_d^{PMCA}$ ( $\mu$ M)	179.9 (129–349)	
$Ca_{50}^{PMCA}$ (nM)	66.5	42.1
$k_{Leak}^{RyR}$ (s $^{-1}$ )	Assumed 0	0.035 (0.007–0.041)

Data are expressed as mean (95% CI). See Fig. 10 B.



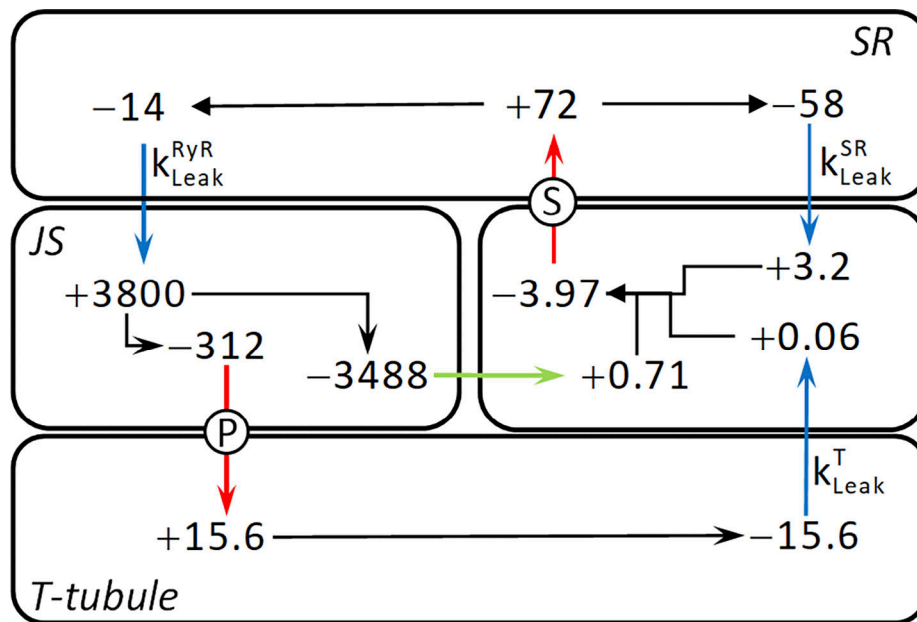


Figure 9. **Summary of steady-state  $\text{Ca}^{2+}$  flows.** Flows of  $\text{Ca}^{2+}$  between compartments of the model fiber are indicated by arrows and quantified by flow rates in  $\mu\text{M s}^{-1}$ . Arrow colors: blue, passive leaks; red, active pumps; green, diffusion; black, division of flows within compartments. Pumps: P, PMCA; S, SERCA. Leaks are identified by adjacent leak rate constant symbols. Rates in each compartment are expressed with concentrations relative to that compartment's volume; -, efflux from a compartment; +, influx into a compartment. Differences in rates between the ends of arrows that span compartment boundaries reflect the difference in volumes of the two compartments. The following values were used to construct the diagram:  $\text{Ca}_{\text{SR}}$ , 400  $\mu\text{M}$ ;  $\text{Ca}_{\text{T}}$ , 1,200  $\mu\text{M}$ ;  $k_{\text{Leak}}^{\text{T}}$ , 0.013  $\text{s}^{-1}$ ;  $k_{\text{Leak}}^{\text{RyR}}$ , 0.035  $\text{s}^{-1}$ ; and  $k_{\text{Leak}}^{\text{SR}}$ , 0.145  $\text{s}^{-1}$ .

of the magnitude given in Table 5. In the absence of a leak of  $\text{Ca}^{2+}$  into the JS through the RYRs,  $\text{Ca}_{\text{JS}}$  stayed close to its initial value of 67 nM throughout the period over which the t-system accumulated  $\text{Ca}^{2+}$  (blue line, Fig. 8 B). That constancy reflected the buffering of  $\text{Ca}^{2+}$  by EGTA and diffusion of  $\text{Ca}^{2+}$  into the JS from the myoplasm. In the presence of a leak of  $\text{Ca}^{2+}$  into the JS,  $\text{Ca}_{\text{JS}}$  increased toward  $\sim 100$  nM (red line, Fig. 8 B). In Fig. 8 C, the time courses are shown of  $\text{Ca}^{2+}$  entering the SR and t-system and binding to buffers in the SR. Note that when  $\text{Ca}_{\text{M}}$  is 67 nM, the rate at which SERCA operates is  $\sim 1\%$  of its maximum, so the filling of the SR is relatively slow. In the SR, most  $\text{Ca}^{2+}$  binds rapidly to the SR buffers (magenta curve, Fig. 8 C). The buffer characteristics allow  $\text{Ca}_{\text{SR}}$  to increase rapidly at the start of filling (green curve, Fig. 8 C), thus stimulating the RYR  $\text{Ca}^{2+}$  leak when tetracaine is not present. The t-system begins to fill immediately, fueled initially by the free  $\text{Ca}^{2+}$  in equilibrium with EGTA in the JS when the protocol begins. In the absence of tetracaine, t-system filling is enhanced by the rise in  $\text{Ca}_{\text{JS}}$  due to the RYR leak (compare with tetracaine [blue curve] to without tetracaine [red curve]; Fig. 8 C).

#### How precisely can the RYR $\text{Ca}^{2+}$ leak be quantified?

A benefit of using the curve-fitting approach to quantifying the RYR leak is that the parameters derived from the fitting procedure can be used to calculate confidence intervals (CIs) for the model parameters whose values were determined from the fitting procedure. Taking the data obtained in the absence of tetracaine as an example and using the raw data points when fitting the model to the data (Fig. 10 A), a confidence contour can be calculated (Motulsky and Christopoulos, 2004). The

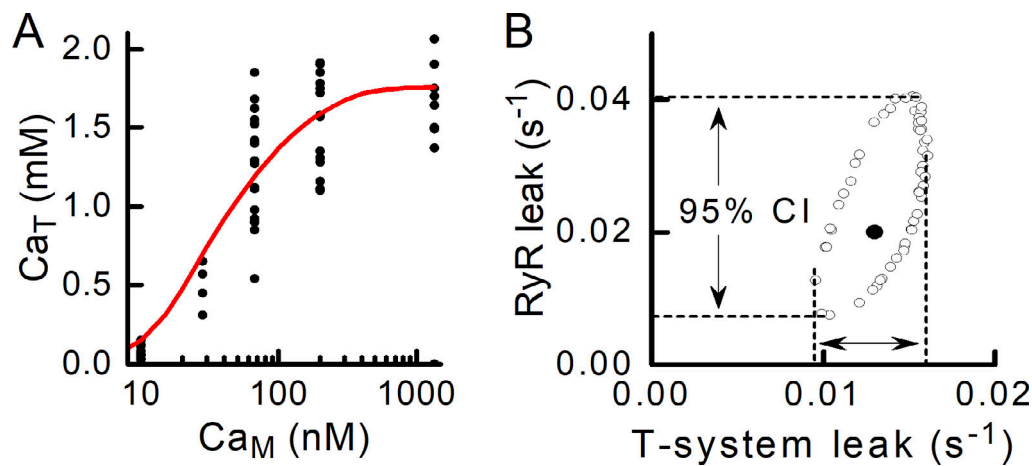
confidence contour is an ellipse (outlined by open circles, Fig. 10 B) that encompasses combinations of parameter values that would give rise to a curve that would not differ significantly, at the 5% level in this case, from the best-fit curve. The parameter combination that gave the best fit is indicated by the solid symbol in the middle of the ellipse (Fig. 10 B, filled circle). The extent of the excursion of the ellipse gives the 95% CI for each parameter, indicated by the dashed lines.

The 95% CI for the RYR leak rate constant is 0.007–0.041  $\text{s}^{-1}$ . The interval excludes 0, which indicates that the method used to quantify the RYR leak was sufficiently sensitive to detect the leak that occurred in the human skinned fibers. The 95% CI would likely be narrowed if data points were obtained at additional  $\text{Ca}_{\text{M}}$  values on the sloping part of the  $\text{Ca}_{\text{T}}$ – $\text{Ca}_{\text{M}}$  curve.

The 95% CIs for  $k_{\text{Leak}}^{\text{T}}$  can be determined in the same way (Fig. 10 B and Table 4). In this case, the 95% CIs for the data with and without tetracaine do not overlap, so it can be concluded that the t-system  $\text{Ca}^{2+}$  leak rate differed significantly depending on whether the RYRs were functional. That is, when  $\text{Ca}^{2+}$  entered the JS through the RYRs, the leak of  $\text{Ca}^{2+}$  from the t-system was reduced compared with that occurring when  $\text{Ca}_{\text{JS}}$  was held constant by the EGTA buffering.

#### Plotting $\text{Ca}_{\text{T}}$ versus $\text{Ca}_{\text{M}}$ or $\text{Ca}_{\text{JS}}$ ?

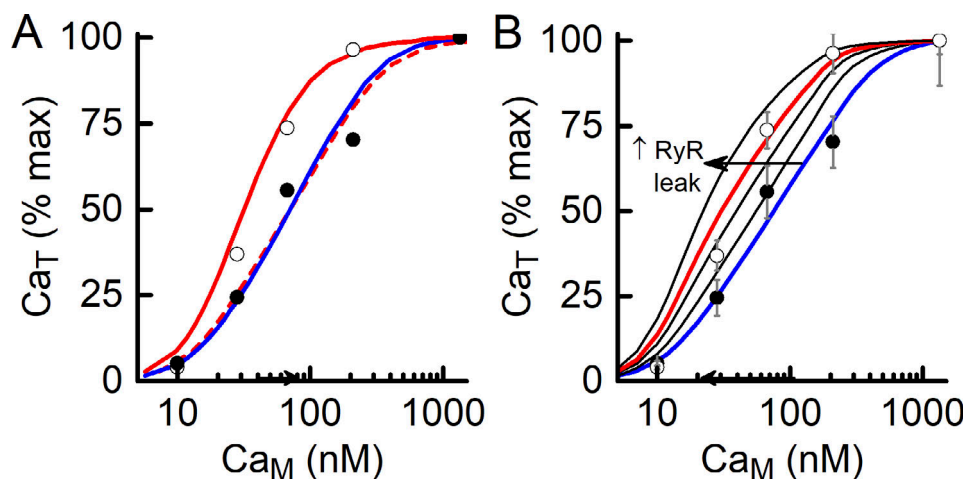
The convention adopted by Launikonis and colleagues (Cully et al., 2016; Cully et al., 2018) is to plot the extent of t-system  $\text{Ca}^{2+}$  accumulation as a function of  $\text{Ca}_{\text{M}}$ . The t-system filling is driven by the PMCA and so must reflect  $\text{Ca}_{\text{JS}}$  rather than  $\text{Ca}_{\text{M}}$ . However,  $\text{Ca}_{\text{JS}}$  is unknown; hence the practice of using  $\text{Ca}_{\text{M}}$  as the independent variable. The model provides the means to



**Figure 10. Confidence interval for RYR leak.** (A) The raw data (filled circles; 63 data points from 17 fibers) obtained without tetracaine present were fitted with a model-derived curve (solid line) from which the best-fit values of  $k_{\text{Leak}}^{\text{T}}$  and  $k_{\text{Leak}}^{\text{RyR}}$  were determined. Knowing the minimum sum of squared residuals (from the best fit), a larger sum of squared residuals can be calculated that would reflect a parameter combination that would give a significantly different curve from the best fit curve (Motulsky and Christopoulos, 2004). (B) The ellipse delimited by open circles is the 95% confidence contour: combinations of the two parameters ( $k_{\text{Leak}}^{\text{RyR}}$  and  $k_{\text{Leak}}^{\text{T}}$ ) that lie within the ellipse produce  $\text{Ca}_T$ - $\text{Ca}_M$  curves that do not differ significantly (i.e.,  $P > 0.05$ ) from the best-fit curve. The filled circle is the  $k_{\text{Leak}}^{\text{T}}$  and  $k_{\text{Leak}}^{\text{RyR}}$  combination that gave the best fit of the model to the data. The 95% CIs for each parameter are indicated by the arrows. CIs: RYR leak rate constant, 0.007–0.041  $\text{s}^{-1}$ ; and t-system leak rate constant, 0.009–0.016  $\text{s}^{-1}$ .

estimate  $\text{Ca}_{\text{JS}}$ , and in Fig. 11 A, a comparison is shown of steady-state  $\text{Ca}_T$  values plotted against  $\text{Ca}_M$  and the model-derived  $\text{Ca}_{\text{JS}}$ . For this comparison, the effect of the change in  $k_{\text{Leak}}^{\text{T}}$  has been removed from the comparison by normalizing steady-state  $\text{Ca}_T$  values obtained with and without tetracaine data by their respective maxima (i.e., values at  $\text{Ca}_M$  of 1,340 nM). When plotted as a function of  $\text{Ca}_M$ , the effect of withdrawing tetracaine, thus allowing the RYR  $\text{Ca}^{2+}$  leak, is to shift the normalized  $\text{Ca}_T$ - $\text{Ca}_M$  relationship to the left. This effect is eliminated when  $\text{Ca}_T$  is plotted against  $\text{Ca}_{\text{JS}}$ ; in that case, the two curves (solid blue and

dashed red lines, Fig. 11 A) superimpose. Remembering that changes in  $k_{\text{Leak}}^{\text{T}}$  have been excluded from this analysis, the observation that the  $\text{Ca}_T$ - $\text{Ca}_{\text{JS}}$  curve overlies the  $\text{Ca}_T$ - $\text{Ca}_M$  curve in the presence of tetracaine, is important because it confirms (1) that the PMCA properties are unaffected by the presence of tetracaine, (2) that t-system filling simply reflects the combined properties of PMCA and the t-tubule  $\text{Ca}^{2+}$  leak, and (3) that the shift of the  $\text{Ca}_T$ - $\text{Ca}_M$  curve to the left when tetracaine is removed from the fibers reflects the increase in  $\text{Ca}_{\text{JS}}$  in the presence of RYR  $\text{Ca}^{2+}$  leak. The last point highlights the benefit of using  $\text{Ca}_M$



**Figure 11. Effect of RYR  $\text{Ca}^{2+}$  leak on  $\text{Ca}_T$ - $\text{Ca}_M$  relationship.** (A) Comparison of curves relating  $\text{Ca}_T$  to  $\text{Ca}_M$  or  $\text{Ca}_{\text{JS}}$ . Symbols show experimental data in the presence (filled circles) and absence (open circles) of tetracaine. The curves are the best fits of the model to the data (blue, with tetracaine; red, without tetracaine). In the presence of a leak of  $\text{Ca}^{2+}$  through the RYRs into the JS (i.e., no tetracaine), the plot of  $\text{Ca}_T$ - $\text{Ca}_M$  is shifted to the left (red solid line) of the case with no RYR leak (blue line). If the curve in the presence of a leak is plotted against the model-derived steady-state  $\text{Ca}_{\text{JS}}$ , the curve (red dashed line) superimposes on that for no RYR leak. (B) Effect of magnitude of the rate constant for RYR  $\text{Ca}^{2+}$  leak on the relationship between steady-state  $\text{Ca}_T$  and  $\text{Ca}_M$ . The blue curve is that for no RYR  $\text{Ca}^{2+}$  leak (e.g., in the presence of tetracaine), and the other curves are for leak rate constants of (from right to left) 0.01, 0.02, 0.03 (red), and 0.04  $\text{s}^{-1}$ . The horizontal separation between the curves with and without RYR  $\text{Ca}^{2+}$  leak increases as leak rate increases (direction indicated by arrow).

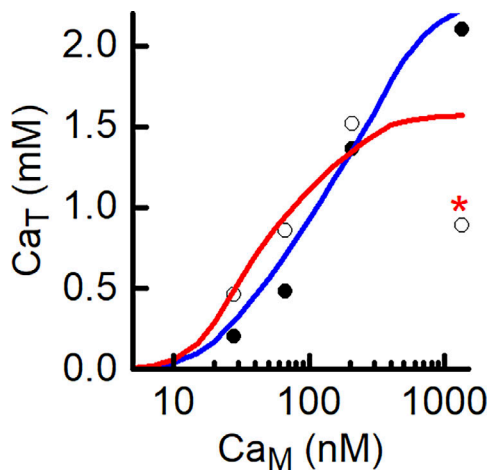


Figure 12. **Modeling MH-susceptible fibers.** Experimental data (symbols: filled circles, with tetracaine; open circles, without tetracaine) from human muscle fibers containing an MH causative mutation of the RYRs. Curves (blue, with tetracaine; red, without tetracaine) show the best fit of the model to the experimental data. Note, point marked with an asterisk was omitted from the analysis (for explanation, see Results). The best-fit value of  $k_{\text{Leak}}^{\text{RyR}}$  was  $0.08 \text{ s}^{-1}$ .

as the independent variable: the size of the horizontal difference between the normalized curves reflects the magnitude of the  $\text{Ca}^{2+}$  leak into the JS, as illustrated in Fig. 11 B.

### Applying the model to data from fibers with malignant hyperthermia (MH)-causative RYR mutation

Cully et al. (2018) measured  $\text{Ca}_T$ - $\text{Ca}_M$  curves for human muscle fibers exhibiting a MH-causative RYR mutation. The model was used to quantify RYR  $\text{Ca}^{2+}$  leak for these fibers. For this analysis, it was recognized that the steady-state  $\text{Ca}_T$  value measured without tetracaine at the highest  $\text{Ca}_M$  (indicated by \* in Fig. 12) is much lower than the point at the next lowest  $\text{Ca}_M$ . Cully et al. (2018) suggested that this reflected activation of store-operated calcium entry (SOCE), which occurred only at the highest  $\text{Ca}_M$  used. No SOCE mechanism was included in the model, so the unusual data point was excluded from the curve-fitting procedure. The model analysis indicated that  $K_D^{\text{PMCA}}$  was twofold higher in the MH fibers ( $385 \mu\text{M}$ , corresponding to  $\text{Ca}_{50}^{\text{PMCA}} = 72 \text{ nM}$ ) than in the control fibers (Table 5) and that  $k_{\text{Leak}}^{\text{RyR}}$  was  $0.08 \text{ s}^{-1}$ , more than twice as great as that for fibers without the MH pathology (Table 5). If SR function is otherwise unaltered by the RYR mutation, then the model indicates that  $\text{Ca}_{\text{SR}}$  would be little affected by the greater RYR leak (i.e., SR  $\text{Ca}^{2+}$  is well buffered). The absolute  $\text{Ca}^{2+}$  leak, assuming  $\text{Ca}_{\text{SR}}$  is  $400 \mu\text{M}$ , would be  $\sim 32 \mu\text{M s}^{-1}$ . Thus, RYR  $\text{Ca}^{2+}$  fluxes in resting muscle fibers are not fixed but rather can be modulated by functional alterations to the RYRs.

## Discussion

The model accurately predicted  $\text{Ca}^{2+}$  accumulation by the t-system in the skinned fiber preparation. It predicted the form of the  $\text{Ca}_T$ - $\text{Ca}_M$  relationship (Figs. 4 B and 8 A), the effect of tetracaine on that relationship (Fig. 8 A), and the time course with which  $\text{Ca}^{2+}$  accumulates in the t-system (Fig. 5 D). This was

achieved with most parameter values determined from information in the literature. The only parameters that required fine-tuning to align the model to the experimental data were the rate constants for  $\text{Ca}^{2+}$  leaks from the t-system into the myoplasm and from the SR into the JS and the  $\text{Ca}^{2+}$  sensitivity of the PMCA, for which values were unknown. The experimental design used by Cully et al. (2018) sought to identify the presence of a  $\text{Ca}^{2+}$  leak through the SR  $\text{Ca}^{2+}$  release channels by comparing the steady-state  $\text{Ca}_T$ - $\text{Ca}_M$  relationships obtained in the presence and absence of the RYR inhibitor tetracaine. From simple observation of the  $\text{Ca}_T$ - $\text{Ca}_M$  curves with and without tetracaine, it was difficult to clearly establish whether the relationship altered as would be expected if there was a flow of  $\text{Ca}^{2+}$  through the RYRs, because a decrease in the t-system  $\text{Ca}^{2+}$  leak alone would also shift the relationship to the left. However, with the available experimental data, the statistical sensitivity of the model-based determination of the RYR leak was adequate to establish that there was a leak through the RYRs in the absence of the RYR blocker, and its magnitude was calculated. Furthermore, use of the model enabled the rate of  $\text{Ca}^{2+}$  leak from the t-system to be quantified, in both the presence and absence of RYR leak.

It was important to ensure that the calculated magnitude of the leak was not dependent on the choice of parameter values. The sensitivity analysis indicated that the parameters with most influence on t-system  $\text{Ca}^{2+}$  accumulation were, perhaps not surprisingly, those directly associated with the t-system. The value of only one of those, PMCA concentration, was set at a predetermined value. If the pump concentration was different from that assumed, fitting the model to the data would give different values for  $k_{\text{Leak}}^{\text{T}}$  and  $K_d^{\text{PMCA}}$ , but the value of  $k_{\text{Leak}}^{\text{RyR}}$  would be unaltered.

JS volume influences the estimated value of  $k_{\text{Leak}}^{\text{RyR}}$  as indicated by the sensitivity analysis (Table 4). JS volume is difficult to quantify because the region is a conceptual, rather than physically defined, space. Its assumed volume is important in the model in that it determines how much  $\text{Ca}_{\text{JS}}$  increases for a given RYR  $\text{Ca}^{2+}$  leak. If a larger JS volume is assumed, then a faster RYR  $\text{Ca}^{2+}$  leak is required to produce the observed steady-state  $\text{Ca}_T$ . The magnitude of the effect, however, is not great: if JS volume was 50% greater than the value used, then  $k_{\text{Leak}}^{\text{RyR}}$  determined from the curve fitting would be increased by  $\sim 12\%$ . Overall, our estimate of  $k_{\text{Leak}}^{\text{RyR}}$  seems fairly robust.

### A framework for interpretation of experimental data

The analysis presented in Results provides a framework for interpreting the  $\text{Ca}_T$ - $\text{Ca}_M$  relationship. In Fig. 13, the effects of a RYR leak, a change in t-system  $\text{Ca}^{2+}$  leak and the combined effects are illustrated. The presence of a RYR  $\text{Ca}^{2+}$  leak is evident through a pure leftward shift of the relationship determined in the absence of tetracaine compared with that in the presence of tetracaine (Fig. 13 A). Changes in the rate of leak of  $\text{Ca}^{2+}$  from the t-system upon the removal of tetracaine are evident as a vertical shift in steady-state  $\text{Ca}_T$  values (Fig. 13 B). If  $k_{\text{Leak}}^{\text{T}}$  decreases, steady-state  $\text{Ca}_T$  values increase, and conversely, if  $k_{\text{Leak}}^{\text{T}}$  increases,  $\text{Ca}_T$  values will decrease. When there is both an RYR leak and a change in t-system  $\text{Ca}^{2+}$  leak, the two effects can be difficult to distinguish by observation alone (Fig. 13 C). The

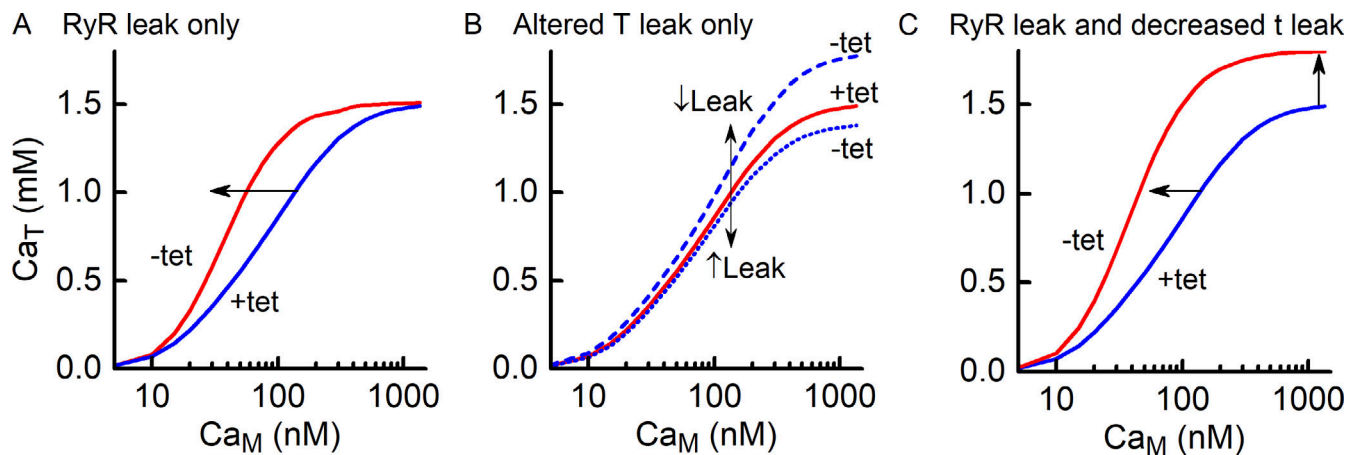


Figure 13. **A framework for interpreting tetracaine-dependent changes in  $Ca_T$ - $Ca_M$  curves.** (A) If withdrawal of tetracaine is accompanied by onset of a  $Ca^{2+}$  leak through the RyRs, the steady state  $Ca_T$ - $Ca_M$  curve is shifted leftward, as indicated by the arrow. (B) If withdrawal of tetracaine is accompanied by a decrease in  $k_{leak}^T$  and no RyR leak, then the  $Ca_T$ - $Ca_M$  curve shifts upward if  $k_{leak}^T$  decreases (blue dashed curve) or downward if  $k_{leak}^T$  increases (blue dotted curve). (C) If withdrawal of tetracaine results in onset of an RyR  $Ca^{2+}$  leak and a decrease in  $k_{leak}^T$ , then the  $Ca_T$ - $Ca_M$  curve is shifted leftward and upward.

model curve-fitting procedure described here allows the RyR and t-system  $Ca^{2+}$  leaks to be identified and quantified.

Measurements of t-system filling with  $Ca_M$  set to 1,340 nM provide important information. That  $Ca^{2+}$  concentration exceeds that required to fully activate PMCA. As shown in Fig. 3 B (curve c), the rate of  $Ca^{2+}$  pumping by PMCA reaches its maximum at  $\sim 400$  nM. Therefore, if  $Ca_M$  is  $>400$  nM, any increase in  $Ca_{JS}$  due to RyR leak will have no effect on the rate of  $Ca^{2+}$  pumping by PMCA or on steady-state  $Ca_T$ . This is evident from the absence of correlation between  $k_{Leak}^{RyR}$  and steady-state  $Ca_T$  when  $Ca_M$  is 1,340 (Table 4). Thus, the tetracaine dependence of steady-state  $Ca_T$  measured at 1,340 nM reflects changes in only  $k_{Leak}^T$ , unsullied by  $k_{Leak}^{RyR}$ : an increase in  $Ca_T$  shows that  $k_{Leak}^T$  has decreased, whereas a decrease shows that  $k_{Leak}^T$  has increased. This is important because, as described earlier (see Fig. 12), Cully et al. (2018) showed that in fibers from people with a susceptibility to MH, steady-state  $Ca_T$  at  $Ca_M$  of 1,340 nM was markedly reduced when measured in the absence of tetracaine compared with that when measured in the presence of tetracaine. This is consistent with a substantial increase in  $k_{Leak}^T$ , most likely via activation of SOCE, independent of any changes in RyR leak, at least when  $Ca_{JS}$  is high.

#### How much could RyR $Ca^{2+}$ leak contribute to resting metabolism?

The cycling of  $Ca^{2+}$  between the SR and myoplasm requires SERCA to move the  $Ca^{2+}$  into the SR. SERCA consumes ATP, which will be regenerated by oxidative phosphorylation in the mitochondria. In a resting muscle in a metabolic steady state, the net heat production arises from the oxidative regeneration of ATP used by SERCA. The SERCA-related heat production associated with the calculated  $Ca^{2+}$  fluxes shown in Fig. 9 can be calculated on the basis of a  $Ca^{2+}$ :ATP stoichiometry of 2 and the production of 74 mJ ( $\mu\text{mol ATP}$ ) $^{-1}$  (see Introduction). If resting  $Ca_M$  is stable (Carroll et al., 1995) in the face of a continual flux of  $Ca^{2+}$  from the SR into the myoplasm, then  $Ca^{2+}$  must be removed from the myoplasm at the same rate

that it enters. From Fig. 9, the RyR efflux of  $Ca^{2+}$  from the SR was 14  $\mu\text{M s}^{-1}$ . To balance that flow, taking account of the relative volumes, this would require SERCA to remove  $Ca^{2+}$  from the myoplasm at 0.77  $\mu\text{M s}^{-1}$ , using ATP at half that rate, 0.39  $\mu\text{M s}^{-1}$ . The associated rate of heat production would be 74 mJ  $\mu\text{mol}^{-1} \times 0.39 \mu\text{mol liter}^{-1} \text{s}^{-1} = 29 \text{ mW kg}^{-1}$ . With the scheme shown in Fig. 9, 8% of the RyR  $Ca^{2+}$  leak is pumped into the t-system before leaking into the myoplasm and being returned to the SR via SERCA; that is, this component is pumped twice in each  $Ca^{2+}$  leak/uptake cycle. This would increase the heat production associated with the RyR  $Ca^{2+}$  leak by 8%, to 31  $\text{mW kg}^{-1}$ .

In comparison, the estimated resting heat production in human forearm muscle is 600  $\text{mW kg}^{-1}$  (Table 1), so the RyR  $Ca^{2+}$  leak component is  $100 \times 31/600 = 5\%$  of muscle resting heat production. The magnitude of this value is consistent with an experimental determination. Chinnet et al. (1992) determined the contribution of PMCA to resting heat production of mouse slow-twitch muscle by measuring the decrease in muscle heat production when PMCA was blocked by pharmacological inhibition of calmodulin. It can be difficult to interpret the results of experiments involving blocking part of the  $Ca^{2+}$  cycling process, but their results were similar to the current analysis: PMCA accounted for 3.2% of resting heat production. Together with the current estimate, this supports the idea that under normal physiological conditions and in the absence of pathological alterations in  $Ca^{2+}$  handling, RyR  $Ca^{2+}$  leak makes only a small contribution to skeletal muscle resting metabolism. However, it is clear that RyR  $Ca^{2+}$  flux can vary across a huge range. The  $Ca^{2+}$  leak calculated in Results for MH fibers was 2.3 times greater than that for fibers with no RyR pathology and thus could be expected to produce  $\geq 60 \text{ mW kg}^{-1}$ , which could increase muscle resting metabolism by 5%. At the other extreme to the leak in resting fibers, in response to stimulation, SR  $[Ca^{2+}]$  decreases at rates of up to 50  $\text{mM s}^{-1}$  (Sztretzky et al., 2011a),  $>3,000$  times greater than the leak measured in resting fibers.



Table A1. **Model equations**

<b>Buffering</b>	
SR	$\frac{dCa_B}{dt} = k_{on}^B \cdot Ca_{SR}(t)^n \cdot (B_{Tot} - Ca_B) - k_{off}^B \cdot Ca_B$
Myoplasm	$\frac{dCaEGTA_M}{dt} = k_{on}^{EGTA} \cdot Ca_M(t) \cdot (EGTA_{Tot} - CaEGTA_M) - k_{off}^{EGTA} \cdot CaEGTA_M$
JS	$\frac{dCaEGTA_{JS}}{dt} = k_{on}^{EGTA} \cdot Ca_{JS}(t) \cdot (EGTA_{Tot} - CaEGTA_{JS}) - k_{off}^{EGTA} \cdot CaEGTA_{JS}$
<b>Leaks</b>	
From t-system	$k_{Leak}^T \cdot (Ca_T(t) - Ca_M(t))$
From SR, via RYR	$k_{Leak}^{RyR} \cdot (Ca_{SR}(t) - Ca_{JS}(t))$
From SR, non-RYR	$k_{Leak}^{SR} \cdot (Ca_{SR}(t) - Ca_M(t))$
Diffusion	$k_{Diff} \cdot (Ca_{JS}(t) - Ca_M(t))$
<b>Combined differential equations</b>	
$\frac{dCa_T}{dt} = \frac{V_{JS}}{V_T} \cdot M_{PMCA}(Ca_J, Ca_T, K_D^{PMCA}, c_{PMCA}) - k_{Leak}^T \cdot (Ca_T(t) - Ca_M(t))$	
$\frac{dCa_{SR}}{dt} = \frac{V_M}{V_{SR}} \cdot M_{SERCA}(Ca_M, Ca_{SR}, K_D^{SERCA}, c_{SERCA}) - k_{Leak}^{RyR} \cdot (Ca_{SR}(t) - Ca_{JS}(t)) - k_{Leak}^{SR} \cdot (Ca_{SR}(t) - Ca_M(t)) - \frac{dCa_B}{dt}$	
$\frac{dCa_{JS}}{dt} = \frac{V_{SR}}{V_{JS}} \cdot k_{Leak}^{RyR} \cdot (Ca_{SR}(t) - Ca_{JS}(t)) - \frac{dCa_T}{dt} - \frac{dCaEGTA_{JS}}{dt} - k_{diff} \cdot (Ca_{JS}(t) - Ca_M(t))$	
$\frac{dCa_M}{dt} = \frac{V_{SR}}{V_M} \cdot k_{Leak}^{SR} \cdot (Ca_{SR}(t) - Ca_M(t)) + \frac{V_T}{V_M} \cdot k_{Leak}^T \cdot (Ca_T(t) - Ca_M(t)) + \frac{V_{JS}}{V_M} \cdot k_{diff} \cdot (Ca_{JS}(t) - Ca_M(t)) - M_{SERCA}(Ca_M, Ca_{SR}, K_D^{SERCA}, c_{SERCA}) - \frac{dCaEGTA_M}{dt}$	

### Non-RYR Ca<sup>2+</sup> leak from the SR

The experimental evidence presented by [Chinet et al. \(1992\)](#) indicated that ~25% of resting metabolism is related to SERCA activity. The simplest interpretation of this observation is that there is a continual leak of Ca<sup>2+</sup> from the SR into the myoplasm or JS that is pumped back into the SR with the metabolic cost (as either heat production or O<sub>2</sub> consumption) reflecting the mitochondrial activity required to support SERCA-related ATP turnover. The current analysis shows that RYR Ca<sup>2+</sup> leak is only one-quarter of the total leak required to account for the SERCA-dependent Ca<sup>2+</sup> leak ([Fig. 9](#)). If this is correct, what accounts for the majority of the leak? Ca<sup>2+</sup> leaks from the SR of resting fibers ([Macdonald and Stephenson, 2001](#); [Lamboley et al., 2014](#)) and from SR vesicles (e.g., [Simonides and Van Hardeveld, 1988](#)) via a mechanism directly involving SERCA. These leaks were not associated with the normal pump cycle and thus are not related to pump reversal or uncoupling (both unlikely under physiological conditions of low myoplasmic Ca<sup>2+</sup> and SR free [Ca<sup>2+</sup>] of ~500 μM). In fact, a leak mechanism, independent of the ATP-splitting pump cycle, seems to be a characteristic of SERCA ([Jilka et al., 1975](#)); [Berman \(2001\)](#) has described this as “channel-like behavior.”

[Lamboley et al. \(2014\)](#) reported that the SERCA-related Ca<sup>2+</sup> leak in skinned human fibers was 6–8 μM s<sup>-1</sup> (recalculated from the original data to express concentrations with respect to myoplasmic volume, allowing direct comparison with values in [Fig. 9](#)). That was measured at pH 8.5, which those authors suggested would increase the leak compared with that at physiological pH. In that case, those values are probably in reasonable agreement with the 3.2 μM s<sup>-1</sup> from the current analysis ([Fig. 9](#)) that arises from the assumption that 25% of resting metabolism

arises from Ca<sup>2+</sup> cycling. Therefore, it would appear that assumption is not unreasonable, and given the relative magnitudes of the RYR and SERCA Ca<sup>2+</sup> leaks, a comprehensive investigation of the role of Ca<sup>2+</sup> cycling in resting metabolism of skeletal muscle should include both leak pathways.

### Conclusion

The model developed for this study can accurately predict the characteristics of t-system Ca<sup>2+</sup> accumulation and can be used to quantify the Ca<sup>2+</sup> leak through the RYRs. The main analysis used data from human muscle fibers with no Ca<sup>2+</sup> handling-related pathology. In these fibers, there is only a small flux of Ca<sup>2+</sup> through the RYRs when the fibers are unstimulated. However, RYR Ca<sup>2+</sup> fluxes can potentially vary greatly. For example, in resting fibers, larger RYR fluxes occur in pathological states, such as MH ([Cully et al., 2018](#)), and in muscle from mice developed to study variations in RYR function ([Lamboley et al., 2021](#)). It is apparent from the Ca<sub>T</sub>–Ca<sub>M</sub> relationships published in those papers that there are changes with genotype in not only  $k_{Leak}^{RyR}$  but also  $k_{Leak}^T$  and  $K_D^{PMCA}$ . The current model provides a means by which these changes can be distinguished and quantified.

The heat generated, mostly by SERCA, in balancing the small RYR leak is only a small fraction of the resting metabolic rate of skeletal muscle. Although Ca<sup>2+</sup> pumped into the t-system by PMCA is used by [Launikonis and colleagues](#) as a biosensor, it is unlikely that PMCA contributes greatly to muscle heat production. As illustrated in [Fig. 9](#), because of the relatively small amount of PMCA compared with SERCA, the majority of Ca<sup>2+</sup> that leaks into the JS will be removed from the myoplasm into the SR via SERCA, and that will be the source of most of the heat

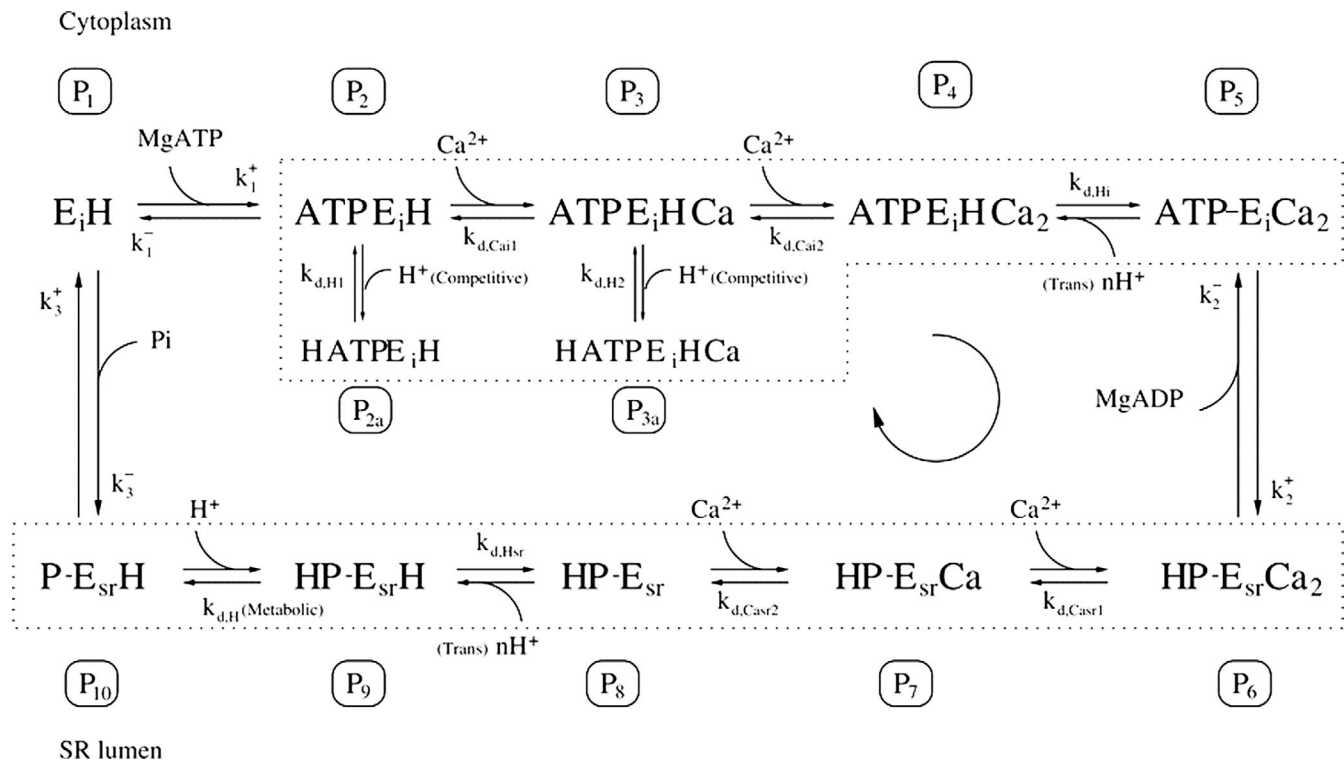


Figure A1. **Schematic of biochemical model of SERCA.** The eight-state model of Ca<sup>2+</sup> transport by SERCA described by Tran et al. (2009). This was a simplification of a 12-state model and underlies their 2-state model, as used in the current study. Rate constants are indicated by  $k_x^+$  or  $k_x^-$  for forward and reverse reactions, respectively, and  $x$  can be 1, 2, or 3, as shown in the figure). Dissociation constants are depicted by  $k_d$ . The figure is reproduced from Tran et al. (2009).

production. In the current context, the discrete localization of PMCA in the JS, allied with the protocol of comparing t-system Ca<sup>2+</sup> accumulation in the presence and absence of an RYR inhibitor and a quantitative model, makes for an extremely sensitive sensor of Ca<sup>2+</sup> movement through the RYR in resting muscle.

The current model was a development of a previous one that was used to predict Ca<sup>2+</sup> movements and heat production in intact muscle fibers in response to stimulation (Bakker et al., 2017; Barclay and Launikonis, 2021). The improvements in the current model include an enhanced spatial representation of the fiber, a more physiological model of SERCA, and the inclusion of PMCA. There are more sophisticated models of cellular Ca<sup>2+</sup> handling (e.g., Baylor and Hollingworth, 2007), but a strength of the current approach is the extension from the microscopic Ca<sup>2+</sup> movements within a cell to the macroscopic consequence of those events in terms of heat production. Incorporation of heat production in the model is useful both for comparison with observed values and as a constraint on the parameters of SERCA. Some models of Ca<sup>2+</sup> movements incorporate diffusion of mobile Ca<sup>2+</sup> entities within the fiber (Cannell and Allen, 1984; Baylor and Hollingworth, 1998). This was deemed unnecessary in the current model because the measured variable, the time course of t-system filling, occurs on a scale of tens of seconds, whereas diffusion on an intrafiber scale (i.e., over micrometer distances) occurs on a millisecond time scale. Any effects of diffusion would be obscured by the slow removal of Ca<sup>2+</sup> from the JS by PMCA.

Ultimately, it is the function of intact muscle fibers that is of interest in relation to the heat produced by resting and contracting muscle fibers. Integrating the current skinned fiber model of Ca<sup>2+</sup> movements in resting fibers with our previous model of Ca<sup>2+</sup> movements in intact fibers in response to stimulus-induced Ca<sup>2+</sup> release would be a valuable step on the path to integrate data from skinned fibers into a model that can relate intracellular Ca<sup>2+</sup> movements to the metabolism of resting and active intact muscle fibers.

## Appendix 1

### Model equations and parameter values

The skinned fiber model depicted in Fig. 1 was described mathematically as a set of ordinary differential equations. The equations are listed in Table A1. They are categorized as buffering reactions, those involving EGTA or buffers in the SR, leaks, and combined equations. The latter incorporate all movements in or out of a physical compartment and include corrections for the change in volume moving from one compartment to another. Details of the model used for Ca<sup>2+</sup> pumping by SERCA and PMCA are given in the following section.

### Model parameter values

The model used for SERCA and PMCA was a two-state model (Fig. 2 A) developed by Tran et al. (2009). That was based on an eight-state biochemical model (Fig. A1). The apparent rate

Table A2. Parameter values

Parameter values for Ca <sup>2+</sup> pumps			Rate constants for buffers and diffusion	Concentrations	Rate constants for leaks
Parameter	SERCA	PMCA	Units		
$k_1^+$	25.9		$\mu\text{M}^{-1} \text{s}^{-1}$	$k_{\text{on}}^B/k_{\text{off}}^B$	$1.55 \times 10^{-6} \mu\text{M}^{-1} \text{s}^{-1}/3,000 \text{s}^{-1}$
$k_2^+$	2,540		$\mu\text{M}^{-1} \text{s}^{-1}$	$k_{\text{on}}^{\text{EGTA}}/k_{\text{off}}^{\text{EGTA}}$	$1.67 \mu\text{M}^{-1} \text{s}^{-1}/0.31 \text{s}^{-1}$
$k_3^+$	23.6		$\mu\text{M}^{-1} \text{s}^{-1}$	$k_{\text{diff}}$	$2.8 \times 10^4 \text{s}^{-1}$
$k_1^-$	51.8		$\text{s}^{-1}$		
$k_2^-$	67.2		$\text{s}^{-1}$	[ATP]	$8 \times 10^3 \mu\text{M}$
$k_3^-$	0.149		$\text{s}^{-1}$	[ADP]	$5 \mu\text{M}$
$K_{d,\text{Ca}_i}^*$	3,540	180	$\mu\text{M}$	[Pi]	$1 \times 10^3 \mu\text{M}$
$K_{d,\text{Ca}_{\text{SR}}}$	2,240		$\mu\text{M}$	pH/[H <sup>+</sup> ]	7.1/0.0794
$K_{d,\text{H}_1}$	0.0109		$\mu\text{M}$		
$K_{d,\text{H}_i}$	3,540		$\mu\text{M}$		$k_{\text{Leak}}^T$ Values determined as described in text
$K_{d,\text{H}_{\text{SR}}}$	0.0105		$\mu\text{M}$		$k_{\text{Leak}}^{\text{RVR}}$
$K_{d,\text{H}}$	0.0724		$\mu\text{M}$		$k_{\text{Leak}}^{\text{SR}}$
[pump]	59	58	$\mu\text{M}$		
$n_{\text{Ca}}$	2				

\* $K_{d,\text{Ca}_i}$  in Fig. A1 corresponds to  $K_D^{\text{SERCA}}$  and  $K_D^{\text{PMCA}}$  for SERCA and PMCA, respectively.  $k_3^+$  was adjusted to match experimentally determined pump turnover ( $6 \text{s}^{-1}$ );  $K_{d,\text{Ca}_i}$  was adjusted to match the observed  $\text{Ca}_{50}$  values; other parameter values for Ca<sup>2+</sup> pumps were as determined by Tran et al. (2009).

constants in the two-state model are functions of the rate constants and dissociation constants in the eight-state scheme as indicated in Fig. A1. In normal operation, the reactions proceed in the clockwise direction with fully cooperative binding of two Ca<sup>2+</sup> from the cytoplasm (from state P<sub>2</sub> to P<sub>4</sub>) that are transported across the membrane (P<sub>5</sub> to P<sub>6</sub>) and released into the SR (P<sub>6</sub> to P<sub>8</sub>). Each cycle involves the binding and hydrolysis of ATP, with products ADP and Pi being released at the steps indicated. The model involves H<sup>+</sup> both as part of Ca<sup>2+</sup>/H<sup>+</sup> countertransport and in competition with Ca<sup>2+</sup> binding. The parameter values for the Ca<sup>2+</sup> pump used in the current model are mostly those derived by Tran et al. (2009), with the exception of the Ca<sup>2+</sup> dissociation constant on the myoplasmic side of the pump ( $K_{d,\text{Ca}_i}$  in Fig. A1), which was adjusted to match the empirical  $\text{Ca}_{50}$  values

for SERCA and PMCA (see Materials and methods), and  $k_3^+$ , which was adjusted to match the maximum turnover of the pump to that determined empirically (see Materials and methods). Values of all the parameters for the Ca<sup>2+</sup> pumps, buffer reactions, and concentrations of cellular constituents are given in Table A2.

In terms of the two-state model (see Fig. 2 A), the rate of Ca<sup>2+</sup> translocation by SERCA is

$$M_{\text{SERCA}} = n_{\text{SERCA}} \cdot c_{\text{SERCA}} \cdot \frac{\alpha_1^+ \cdot \alpha_2^+ - \alpha_1^- \cdot \alpha_2^-}{\alpha_1^+ + \alpha_2^+ + \alpha_1^- + \alpha_2^-},$$

where  $\alpha_1^+$  and  $\alpha_2^+$  are the apparent rate constants for the forward transitions between states P<sub>M</sub> and P<sub>SR</sub>, and  $\alpha_1^-$  and  $\alpha_2^-$  are the apparent rate constants for the reverse reactions. The apparent

Table A3. Calculation of apparent rate constants for two-state model of Ca<sup>2+</sup> pumps

$\alpha_1^+ = \frac{k_2^+ \cdot N_{\text{ATP}} \cdot N_{\text{Ca}_i}^2}{N_{\text{ATP}} \cdot (N_{\text{Ca}_i})^2 + N_{\text{H}_i} \cdot (1 + N_{\text{ATP}} \cdot (1 + N_{\text{H}_1} + N_{\text{Ca}_i}^2))}$	$N_{\text{ATP}} = [\text{ATP}]/K_{d,\text{ATP}}$
	$N_{\text{Ca}_i} = \text{Ca}_i/K_{d,\text{Ca}_i}$
	$N_{\text{H}_i} = [\text{H}^+]_i/K_{d,\text{H}_i}$
	$N_{\text{H}_1} = [\text{H}^+]_1/K_{d,\text{H}_1}$
$\alpha_2^+ = \frac{k_3^+ \cdot N_{\text{H}_{\text{SR}}}}{N_{\text{H}_{\text{SR}}} \cdot (1 + N_{\text{H}_i}) + N_{\text{H}} \cdot (1 + N_{\text{Ca}_{\text{SR}}}^2)}$	$N_{\text{H}_{\text{SR}}} = [\text{H}^+]_{\text{SR}}/K_{d,\text{H}_{\text{SR}}}$
	$N_{\text{Ca}_{\text{SR}}} = \text{Ca}_{\text{SR}}/K_{d,\text{Ca}_{\text{SR}}}$
	$N_{\text{H}} = [\text{H}^+]/K_{d,\text{H}}$
$\alpha_1^- = \frac{k_2^- \cdot [\text{ADP}] \cdot N_{\text{Ca}_{\text{SR}}}^2 \cdot N_{\text{H}}}{N_{\text{H}_{\text{SR}}} \cdot (1 + N_{\text{H}_i}) + N_{\text{H}} \cdot (1 + N_{\text{Ca}_{\text{SR}}}^2)}$	$K_{d,\text{ATP}} = \frac{k_1^-}{k_1^+} = \frac{k_2^- \cdot k_3^+ \cdot K_{d,\text{Ca}_{\text{SR}}}^2 \cdot K_{d,\text{H}_1} \cdot K_{d,\text{H}}}{k_2^+ \cdot k_3^+ \cdot K_{d,\text{Ca}_i}^2 \cdot K_{d,\text{H}_{\text{SR}}} \cdot e^{\Delta G_{\text{ATP}}/RT}}$
$\alpha_2^- = \frac{k_3^- \cdot [\text{Pi}] \cdot N_{\text{H}_i}}{N_{\text{ATP}} \cdot N_{\text{Ca}_i}^2 + N_{\text{H}_i} \cdot (1 + N_{\text{ATP}} \cdot (1 + N_{\text{H}_1} + N_{\text{Ca}_i}^2))}$	

Table A4. **Parameter values used for assessing effect of TnC on Ca<sup>2+</sup>-EGTA equilibrium**

Parameter	Value	Comments
EGTA	50,000 $\mu\text{M}$	
$k_{1+}$	$1.67 \text{ M}^{-1} \text{ s}^{-1}$	From $K_d$ of $0.18 \mu\text{M}$ (Smith et al., 1984) and $k_{1-}$
$k_{1-}$	$0.31 \text{ s}^{-1}$	Smith et al. (1984)
TnC	$100 \mu\text{M}$	2 Ca <sup>2+</sup> binding sites/molecule (i.e., binding sites, $200 \mu\text{M}$ )
$k_{2+}$	$240 \text{ M}^{-1} \text{ s}^{-1}$	Baylor et al. (1983) for rabbit TnC, adjusted from $16^\circ\text{C}$ to $25^\circ\text{C}$ assuming a $Q_{10}$ of 2.0
$k_{2-}$	$2,900 \text{ s}^{-1}$	
$k_{3+}$	$4.7 \text{ M}^{-1} \text{ s}^{-1}$	
$k_{3-}$	$165 \text{ s}^{-1}$	

rate constants are functions of the rate constants from the eight-state scheme, the concentrations of ATP and its hydrolysis products, Ca<sup>2+</sup> (on both sides of the SR membrane), H (on both sides of the membrane), and the dissociation constants for the reactions involving those molecules, as indicated in Fig. A1. The formulae for calculating the apparent rate constants are given in Table A3. For further details of the model, see Tran et al. (2009).

## Appendix 2

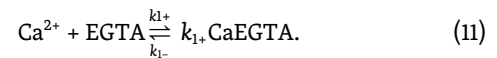
### Ca<sup>2+</sup> binding by EGTA and TnC

An analysis was carried out to see whether Ca<sup>2+</sup> binding by TnC would affect Ca<sup>2+</sup>-EGTA buffering to the extent that free Ca<sup>2+</sup> calculated from considering Ca<sup>2+</sup>-EGTA without taking account of TnC will be inaccurate.

Table A5. **Effect of TnC on Ca<sup>2+</sup> buffering by EGTA**

Unbound [Ca <sup>2+</sup> ] (nM)		Difference	
No TnC	With TnC	nM	%
20	19.999	0.001	0.005
67	66.996	0.004	0.006
200	199.97	0.03	0.015
600	599.69	0.29	0.05
1,000	998.85	1.15	0.11

The binding of Ca<sup>2+</sup> by EGTA was treated as a reversible second-order reaction:



The rate of the reaction is given by the differential equation:

$$\frac{d[\text{CaEGTA}]}{dt} = k_{1+} \cdot \text{Ca}_M(t) \cdot (\text{EGTA}_{\text{Tot}} - \text{CaEGTA}(t)) - k_{1-} \cdot \text{CaEGTA}(t),$$

where EGTA<sub>Tot</sub> is the concentration of EGTA, CaEGTA is the concentration of the product of reaction Eq. 11, Ca<sub>M</sub> is the concentration of unbound Ca<sup>2+</sup> in the myoplasm, and  $k_{1+}$  and  $k_{1-}$  are the rate constants for the forward and backward reactions, respectively.

In fast-twitch mammalian muscle, each TnC molecule binds 2 Ca<sup>2+</sup> in succession.

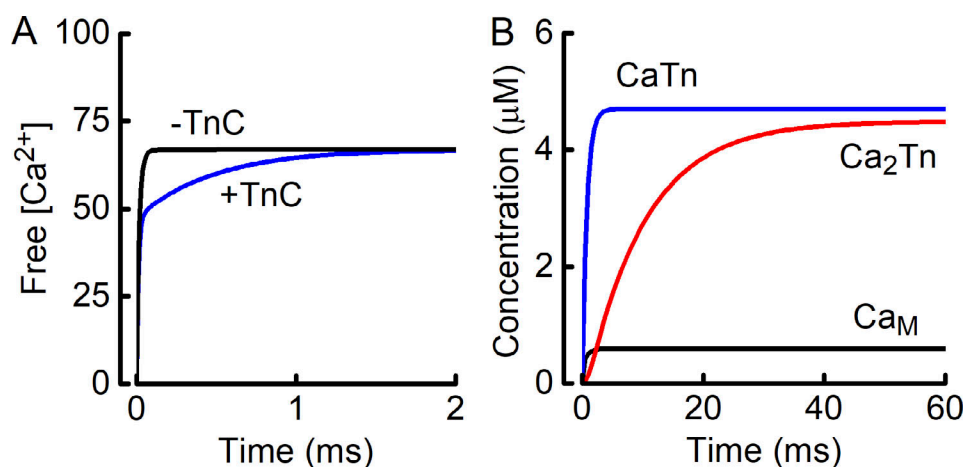
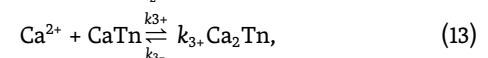
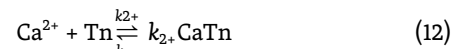


Figure A2. **Analysis of Ca binding by TnC.** (A) Computed time course of establishment of equilibrium between Ca<sup>2+</sup> and EGTA. At time 0, all Ca<sup>2+</sup> bound to EGTA. The kinetic model was used to compute the change in unbound Ca<sup>2+</sup>. The effects of including TnC (labeled +TnC) or considering EGTA alone (-TnC) are shown. In the presence of TnC, equilibration of Ca<sup>2+</sup>-EGTA takes longer (~2 ms), but the eventual free [Ca<sup>2+</sup>] level (67 nM) is the same whether TnC is included or not. (B) Calculated time courses of Ca<sup>2+</sup> binding by TnC. First Ca<sup>2+</sup> binds rapidly (blue) and second Ca<sup>2+</sup> binds more slowly (red). Unbound [Ca<sup>2+</sup>] attains a steady value (600 nM in this example) more rapidly than CaTnC, reflecting the binding kinetics of EGTA. EGTA effectively buffers Ca<sup>2+</sup> even when Ca<sup>2+</sup> is being bound by TnC.



where Tn is TnC, and the rate constants are as shown in the equations. The corresponding differential equations are

$$\frac{dCaTn}{dt} = k_{2+} \cdot Ca_M(t) \cdot (Tn_{Tot} - CaTn(t)) + k_{3-} \cdot Ca_2Tn(t) - k_{2-} \cdot CaTn(t),$$

$$\frac{dCa_2Tn}{dt} = k_{3+} \cdot Ca_M(t) \cdot (CaTn(t) - Ca_2Tn(t)) - k_{3-} \cdot Ca_2Tn(t),$$

where  $Tn_{Tot}$  is the concentration of TnC, CaTn is the concentration of TnC with one  $Ca^{2+}$  bound, and  $Ca_2Tn$  is the concentration of TnC with 2  $Ca^{2+}$  bound. The values of the parameters are given in Table A4. The system of equations was solved, starting with all the  $Ca^{2+}$  bound to EGTA. The analysis involved tracking the temporal evolution of  $Ca_M$ .

In Fig. A2 A, the calculated time course of the (theoretical) increase of  $Ca_M$  as  $Ca^{2+}$  dissociates from EGTA is shown. The time taken for this to occur is affected by TnC, being slower (on a millisecond scale) when TnC is present. The important result is that the final concentration of unbound  $Ca^{2+}$  was not visibly altered by the inclusion of TnC in the model. By comparing the time courses of  $Ca_M$ , CaTn, and  $Ca_2Tn$ , it can be seen that EGTA effectively buffers  $Ca_M$  even while  $Ca^{2+}$  is binding to TnC (Fig. A2 B). The reason for this is that the  $Ca^{2+}$ -EGTA reaction is faster than  $Ca^{2+}$  binding by TnC, so free  $Ca^{2+}$  that binds to TnC is rapidly replaced by  $Ca^{2+}$  dissociating from EGTA.

Close inspection of calculated steady-state  $Ca_M$  values reveals very small differences in  $Ca_M$  depending on whether the effects of TnC are considered (Table A5).  $Ca_M$  is lower when TnC is considered than when it is ignored. However, the magnitude of the difference is small for the range of  $Ca_M$  values used in the current study. For example, when the anticipated  $Ca_M$  is 67 nM, the actual  $Ca_M$ , taking account of the effects of TnC, would be 0.006% lower. The effect is larger for higher values of  $Ca_M$ , reaching 0.1% when  $Ca_M$  is 1  $\mu$ M. For practical purposes, these effects are negligible.

## Acknowledgments

Eduardo Ríos served as editor.

This work was supported by Australian Research Council Discovery Projects grants DP180100937 and DP200100435 and AFM Telethon Research Grant 22181 (to B.S. Launikonis).

The authors declare no competing financial interests.

Author contributions: C. Barclay: Conceptualization, formal analysis, methodology, software, writing—original draft, review and editing. B. Launikonis: Conceptualization, data curation, funding acquisition, project administration, writing—review and editing.

Submitted: 7 July 2021

Accepted: 6 February 2022

## References

Akyempon, C.K., and B.D. Roufogalis. 1982. The stoichiometry of the  $Ca^{2+}$  pump in human erythrocyte vesicles: Modulation by  $Ca^{2+}$ ,  $Mg^{2+}$  and calmodulin. *Cell Calcium*. 3:1–17. [https://doi.org/10.1016/0143-4160\(82\)90034-3](https://doi.org/10.1016/0143-4160(82)90034-3)

Bakker, A.J., T.R. Cully, C.D. Wingate, C.J. Barclay, and B.S. Launikonis. 2017. Doublet stimulation increases  $Ca^{2+}$  binding to troponin C to ensure

rapid force development in skeletal muscle. *J. Gen. Physiol.* 149:323–334. <https://doi.org/10.1085/jgp.201611727>

Barclay, C.J. 2012. Quantifying  $Ca^{2+}$  release and inactivation of  $Ca^{2+}$  release in fast- and slow-twitch muscles. *J. Physiol.* 590:6199–6212. <https://doi.org/10.1113/jphysiol.2012.242073>

Barclay, C.J. 2015. Energetics of contraction. *Comp. Physiol.* 5:961–995. <https://doi.org/10.1002/cphy.c140038>

Barclay, C.J. 2017. Energy demand and supply in human skeletal muscle. *J. Muscle Res. Cell Motil.* 38:143–155. <https://doi.org/10.1007/s10974-017-9467-7>

Barclay, C.J., and B.S. Launikonis. 2021. Components of activation heat in skeletal muscle. *J. Muscle Res. Cell Motil.* 42:1–16. <https://doi.org/10.1007/s10974-019-09547-5>

Barclay, C.J., and D.S. Loiselle. 2020. An equivocal final link—quantitative determination of the thermodynamic efficiency of ATP hydrolysis—sullies the chain of electric, ionic, mechanical and metabolic steps underlying cardiac contraction. *Front. Physiol.* 11:183. <https://doi.org/10.3389/fphys.2020.00183>

Barclay, C.J., R.C. Woledge, and N.A. Curtin. 2007. Energy turnover for  $Ca^{2+}$  cycling in skeletal muscle. *J. Muscle Res. Cell Motil.* 28:259–274. <https://doi.org/10.1007/s10974-007-9116-7>

Barclay, C.J., R.C. Woledge, and N.A. Curtin. 2009. Effects of UCP3 genotype, temperature and muscle type on energy turnover of resting mouse skeletal muscle. *Pflügers Arch.* 457:857–864. <https://doi.org/10.1007/s00424-008-0552-z>

Baylor, S.M., W.K. Chandler, and M.W. Marshall. 1983. Sarcoplasmic reticulum calcium release in frog skeletal muscle fibres estimated from Arsenazo III calcium transients. *J. Physiol.* 344:625–666. <https://doi.org/10.1113/jphysiol.1983.sp014959>

Baylor, S.M., and S. Hollingworth. 1998. Model of sarcomeric  $Ca^{2+}$  movements, including ATP  $Ca^{2+}$  binding and diffusion, during activation of frog skeletal muscle. *J. Gen. Physiol.* 112:297–316. <https://doi.org/10.1085/jgp.112.3.297>

Baylor, S.M., and S. Hollingworth. 2003. Sarcoplasmic reticulum calcium release compared in slow-twitch and fast-twitch fibres of mouse muscle. *J. Physiol.* 551:125–138. <https://doi.org/10.1113/jphysiol.2003.041608>

Baylor, S.M., and S. Hollingworth. 2007. Simulation of  $Ca^{2+}$  movements within the sarcomere of fast-twitch mouse fibers stimulated by action potentials. *J. Gen. Physiol.* 130:283–302. <https://doi.org/10.1085/jgp.200709827>

Berman, M.C. 2001. Slippage and uncoupling in P-type cation pumps; implications for energy transduction mechanisms and regulation of metabolism. *Biochim. Biophys. Acta.* 1513:95–121. [https://doi.org/10.1016/S0005-2736\(01\)00356-x](https://doi.org/10.1016/S0005-2736(01)00356-x)

Cannell, M.B., and D.G. Allen. 1984. Model of calcium movements during activation in the sarcomere of frog skeletal muscle. *Biophys. J.* 45: 913–925. [https://doi.org/10.1016/S0006-3495\(84\)84238-1](https://doi.org/10.1016/S0006-3495(84)84238-1)

Cantilina, T., Y. Sagara, G. Inesi, and L.R. Jones. 1993. Comparative studies of cardiac and skeletal sarcoplasmic reticulum ATPases. Effect of a phospholamban antibody on enzyme activation by  $Ca^{2+}$ . *J. Biol. Chem.* 268: 17018–17025

Carafoli, E. 1991. Calcium pump of the plasma membrane. *Physiol. Rev.* 71: 129–153. <https://doi.org/10.1152/physrev.1991.71.1.129>

Carroll, S.L., M.G. Klein, and M.F. Schneider. 1995. Calcium transients in intact rat skeletal muscle fibers in agarose gel. *Am. J. Physiol. Cell Physiol.* 269:C28–C34. <https://doi.org/10.1152/ajpcell.1995.269.1.C28>

Chinet, A., A. Decrouy, and P.C. Even. 1992.  $Ca^{2+}$ -dependent heat production under basal and near-basal conditions in the mouse soleus muscle. *J. Physiol.* 455:663–678. <https://doi.org/10.1113/jphysiol.1992.sp019321>

Clausen, T., C. Van Hardevel, and M.E. Everts. 1991. Significance of cation transport in control of energy metabolism and thermogenesis. *Physiol. Rev.* 71:733–774. <https://doi.org/10.1152/physrev.1991.71.3.733>

Croisier, H., X. Tan, J.F. Perez-Zoghbi, M.J. Sanderson, J. Sneyd, and B.S. Brook. 2013. Activation of store-operated calcium entry in airway smooth muscle cells: Insight from a mathematical model. *PLoS One.* 8: e69598. <https://doi.org/10.1371/journal.pone.0069598>

Cully, T.R., R.H. Choi, A.R. Bjorksten, D.G. Stephenson, R.M. Murphy, and B.S. Launikonis. 2018. Junctional membrane  $Ca^{2+}$  dynamics in human muscle fibers are altered by malignant hyperthermia causative RyR mutation. *Proc. Natl. Acad. Sci. USA.* 115:8215–8220. <https://doi.org/10.1073/pnas.1800490115>

Cully, T.R., J.N. Edwards, O. Friedrich, D.G. Stephenson, R.M. Murphy, and B.S. Launikonis. 2012. Changes in plasma membrane Ca-ATPase and stromal interacting molecule 1 expression levels for  $Ca^{2+}$  signaling in

- dystrophic mdx mouse muscle. *Am. J. Physiol. Cell Physiol.* 303:C567–C576. <https://doi.org/10.1152/ajpcell.00144.2012>
- Cully, T.R., J.N. Edwards, R.M. Murphy, and B.S. Launikonis. 2016. A quantitative description of tubular system  $\text{Ca}^{2+}$  handling in fast- and slow-twitch muscle fibres. *J. Physiol.* 594:2795–2810. <https://doi.org/10.1113/jp271658>
- Cully, T.R., R.M. Murphy, L. Roberts, T. Raastad, R.G. Fasset, J.S. Coombes, I.D. Jayasinghe, and B.S. Launikonis. 2017. Human skeletal muscle plasmalemma alters its structure to change its  $\text{Ca}^{2+}$ -handling following heavy-load resistance exercise. *Nat. Commun.* 8:14266. <https://doi.org/10.1038/ncomms14266>
- Dulhunty, A.F., P.R. Junankar, and C. Stanhope. 1992. Extra-junctional ryanodine receptors in the terminal cisternae of mammalian skeletal muscle fibres. *Proceedings R. Soc. B.* 247:69–75. <https://doi.org/10.1098/rspb.1992.0010>
- Dzeja, P.P., and A. Terzic. 2003. Phosphotransfer networks and cellular energetics. *J. Exp. Biol.* 206:2039–2047. <https://doi.org/10.1242/jeb.00426>
- Eisenberg, B.R. 1983. Quantitative ultrastructure of mammalian skeletal muscle. In *Handbook of Physiology: Skeletal Muscle*. L.D. Peachey, editor. American Physiological Society, Bethesda, Maryland, USA. 73–112
- Enyedi, A., A.K. Verma, A.G. Filoteo, and J.T. Penniston. 1993. A highly active 120-kDa truncated mutant of the plasma membrane  $\text{Ca}^{2+}$  pump. *J. Biol. Chem.* 268:10621–10626
- Ferguson, D.G., and C. Franzini-Armstrong. 1988. The  $\text{Ca}^{2+}$  ATPase content of slow and fast twitch fibres of guinea pig. *Muscle Nerve.* 11:561–570. <https://doi.org/10.1002/mus.880110607>
- Fischer, H., I. Polikarpov, and A.F. Craievich. 2004. Average protein density is a molecular-weight-dependent function. *Protein Sci.* 13:2825–2828. <https://doi.org/10.1110/ps.04688204>
- Forstea, M.I., F. Soler, and F. Fernandez-Belda. 2001. Unravelling the interaction of thapsigargin with the conformational states of  $\text{Ca}^{2+}$ -ATPase from skeletal sarcoplasmic reticulum. *J. Biol. Chem.* 276:37266–37272. <https://doi.org/10.1074/jbc.m103949200>
- Franzini-Armstrong, C., F. Protasi, and V. Ramesh. 1999. Shape, size, and distribution of  $\text{Ca}^{2+}$  release units and couplons in skeletal and cardiac muscles. *Biophys. J.* 77:1528–1539. [https://doi.org/10.1016/s0006-3495\(99\)77000-1](https://doi.org/10.1016/s0006-3495(99)77000-1)
- Inesi, G., and T.L. Hill. 1983. Calcium and proton dependence of sarcoplasmic reticulum ATPase. *Biophys. J.* 44:271–280. [https://doi.org/10.1016/S0006-3495\(83\)84299-4](https://doi.org/10.1016/S0006-3495(83)84299-4)
- Jayasinghe, I.D., and B.S. Launikonis. 2013. Three-dimensional reconstruction and analysis of the tubular system of vertebrate skeletal muscle. *J. Cell Sci.* 126:4048–4058. <https://doi.org/10.1242/jcs.131565>
- Jayasinghe, I.D., M. Munro, D. Baddeley, B.S. Launikonis, and C. Soeller. 2014. Observation of the molecular organization of calcium release sites in fast- and slow-twitch skeletal muscle with nanoscale imaging. *J. R. Soc. Interf.* 11:20140570. <https://doi.org/10.1098/rsif.2014.0570>
- Jilka, R.L., A.N. Martonosi, and T.W. Tillack. 1975. Effect of the purified  $(\text{Mg}^{2+} + \text{Ca}^{2+})$ -activated ATPase of sarcoplasmic reticulum upon the passive  $\text{Ca}^{2+}$  permeability and ultrastructure of phospholipid vesicles. *J. Biol. Chem.* 250:7511–7524
- Kabo, G.J., O.V. Voitkevich, A.V. Blokhin, S.V. Kohut, E.N. Stepurko, and Y.U. Paulechka. 2013. Thermodynamic properties of starch and glucose. *J. Chem. Thermodynamics.* 59:87–93. <https://doi.org/10.1016/j.jct.2012.11.031>
- Konishi, M. 1998. Cytoplasmic free concentrations of  $\text{Ca}^{2+}$  and  $\text{Mg}^{2+}$  in skeletal muscle fibers at rest and during contraction. *Jap. J. Physiol.* 48:421–438. <https://doi.org/10.2170/jjphysiol.48.421>
- Konishi, M., and M. Watanabe. 1995. Resting cytoplasmic free  $\text{Ca}^{2+}$  concentration in frog skeletal muscle measured with fura-2 conjugated to high molecular weight dextran. *J. Gen. Physiol.* 106:1123–1150. <https://doi.org/10.1085/jgp.106.6.1123>
- Kosk-Kosicka, D., and T. Bzdega. 1988. Activation of the erythrocyte  $\text{Ca}^{2+}$ -ATPase by either self-association or interaction with calmodulin. *J. Biol. Chem.* 263:18184–18189. [https://doi.org/10.1016/s0021-9258\(19\)81342-x](https://doi.org/10.1016/s0021-9258(19)81342-x)
- Kosk-Kosicka, D., and G. Inesi. 1985. Cooperative calcium binding and calmodulin regulation in the calcium-dependent adenosine triphosphatase purified from the erythrocyte membrane. *FEBS Lett.* 189:67–71. [https://doi.org/10.1016/0014-5793\(85\)80843-7](https://doi.org/10.1016/0014-5793(85)80843-7)
- Lamboley, C.R., R.M. Murphy, M.J. McKenna, and G.D. Lamb. 2014. Sarcoplasmic reticulum  $\text{Ca}^{2+}$  uptake and leak properties, and SERCA isoform expression, in type I and type II fibres of human skeletal muscle. *J. Physiol.* 592:1381–1395. <https://doi.org/10.1113/jphysiol.2013.269373>
- Lamboley, C.R., L. Pearce, C. Seng, A. Meizoso-Huesca, D.P. Singh, B.P. Frankish, V. Kaura, H.P. Lo, C. Ferguson, P.D. Allen, et al. 2021. Ryanodine receptor leak triggers fiber  $\text{Ca}^{2+}$  redistribution to preserve force and elevate basal metabolism in skeletal muscle. *Sci. Adv.* 7:eabi7166. <https://doi.org/10.1126/sciadv.abi7166>
- Lee, Y.S., and J.P. Keener. 2008. A calcium-induced calcium release mechanism mediated by calsequestrin. *J. Theor. Biol.* 253:668–679. <https://doi.org/10.1016/j.jtbi.2008.04.027>
- Lytton, J., M. Westlin, S.E. Burk, G.E. Shull, and D.H. MacLennan. 1992. Functional comparison between isoforms of the sarcoplasmic or endoplasmic reticulum family of calcium pumps. *J. Biol. Chem.* 267:14483–14489. [https://doi.org/10.1016/s0021-9258\(19\)49738-x](https://doi.org/10.1016/s0021-9258(19)49738-x)
- Macdonald, W.A., and D.G. Stephenson. 2001. Effects of ADP on sarcoplasmic reticulum function in mechanically skinned skeletal muscle fibres of the rat. *J. Physiol.* 532:499–508. <https://doi.org/10.1111/j.1469-7793.2001.0499f.x>
- Makinose, M., and W. Hasselbach. 1971. ATP synthesis by the reverse of the sarcoplasmic calcium pump. *FEBS Lett.* 12:271–272. [https://doi.org/10.1016/0014-5793\(71\)80196-5](https://doi.org/10.1016/0014-5793(71)80196-5)
- Manno, C., M. Sztretze, L. Figueroa, P.D. Allen, and E. Rios. 2013. Dynamic measurement of the calcium buffering properties of the sarcoplasmic reticulum in mouse skeletal muscle. *J. Physiol.* 591:423–442. <https://doi.org/10.1113/jphysiol.2012.243444>
- Meizoso-Huesca, A., and B.S. Launikonis. 2021. The Orail1 inhibitor BTP2 has multiple effects on  $\text{Ca}^{2+}$  handling in skeletal muscle. *J. Gen. Physiol.* 153:e202012747. <https://doi.org/10.1085/jgp.202012747>
- Mitchell, R.D., A. Saito, P. Palade, and S. Fleischer. 1983. Morphology of isolated triads. *J. Cell Biol.* 96:1017–1029. <https://doi.org/10.1083/jcb.96.4.1017>
- Morrisette, J.M., J.P.G. Franck, and B.A. Block. 2003. Characterization of ryanodine receptor and  $\text{Ca}^{2+}$ -ATPase isoforms in the thermogenic heater organ of blue marlin (*Makaira nigricans*). *J. Exp. Biol.* 206:805–812. <https://doi.org/10.1242/jeb.00158>
- Motulsky, H., and A. Christopoulos. 2004. *Fitting Models to Biological Data Using Linear and Non-Linear Regression*. Oxford University Press, New York. 351 pp.
- Pape, P.C., K. Fenelon, C.R.H. Lamboley, and D. Stachura. 2007. Role of calsequestrin evaluated from changes in free and total calcium concentrations in the sarcoplasmic reticulum of frog cut skeletal muscle fibres. *J. Physiol.* 581:319–367. <https://doi.org/10.1113/jphysiol.2006.126474>
- Park-Holohan, S.J., T.G. West, R.C. Woledge, M.A. Ferenczi, C.J. Barclay, and N.A. Curtin. 2010. Effect of phosphate and temperature on force exerted by white muscle fibres from dogfish. *J. Muscle Res. Cell Motil.* 31:35–44. <https://doi.org/10.1007/s10974-010-9198-5>
- Rolfe, D.F., and G.C. Brown. 1997. Cellular energy utilization and molecular origin of standard metabolic rate in mammals. *Physiol. Rev.* 77:731–758. <https://doi.org/10.1152/physrev.1997.77.3.731>
- Rosenbrock, H.H. 1963. Some general implicit processes for the numerical solution of differential equations. *Computer J.* 5:329–330. <https://doi.org/10.1093/comjnl/5.4.329>
- Sacchetto, R., A. Margreth, M. Pelosi, and E. Carafoli. 1996. Colocalization of the dihydropyridine receptor, the plasma-membrane calcium ATPase isoform 1 and the sodium/calcium exchanger to the junctional-membrane domain of transverse tubules of rabbit skeletal muscle. *Eur. J. Biochem.* 237:483–488. <https://doi.org/10.1111/j.1432-1033.1996.0483k.x>
- Schatzmann, H.J. 1973. Dependence on calcium concentration and stoichiometry of the calcium pump in human red cells. *J. Physiol.* 235:551–569. <https://doi.org/10.1113/jphysiol.1973.sp010403>
- Segal, S.S., T.P. White, and J.A. Faulkner. 1986. Architecture, composition, and contractile properties of rat soleus muscle grafts. *Am. J. Physiol. Cell Physiol.* 250:C474–C479. <https://doi.org/10.1152/ajpcell.1986.250.3.C474>
- Simonides, W.S., and C. Van Hardeveld. 1988.  $(\text{Ca}^{2+} + \text{Mg}^{2+})$ -ATPase activity associated with the maintenance of a  $\text{Ca}^{2+}$  gradient by sarcoplasmic reticulum at submicromolar external  $[\text{Ca}^{2+}]$ . The effect of hypothyroidism. *Biochim. Biophys. Acta.* 943:349–359. [https://doi.org/10.1016/0005-2736\(88\)90567-6](https://doi.org/10.1016/0005-2736(88)90567-6)
- Sjogaard, G., R.P. Adams, and B. Saltin. 1985. Water and ion shifts in skeletal muscle of humans with intense dynamic knee extension. *Am. J. Physiol. Regul. Integr. Comp. Physiol.* 248:R190–R196. <https://doi.org/10.1152/ajpregu.1985.248.2.R190>
- Smith, N.P., C.J. Barclay, and D.S. Loiselle. 2005. The efficiency of muscle contraction. *Prog. Biophys. Mol. Biol.* 88:1–58. <https://doi.org/10.1016/j.pbiomolbio.2003.11.014>
- Smith, P.D., G.W. Liesegang, R.L. Berger, G. Czerlinski, and R.J. Podolsky. 1984. A stopped-flow investigation of calcium ion binding by ethylene glycol bis(beta-aminoethyl ether)-N,N'-tetraacetic acid. *Anal. Biochem.* 143:188–195. [https://doi.org/10.1016/0003-2697\(84\)90575-x](https://doi.org/10.1016/0003-2697(84)90575-x)

- Sneyd, J. 2005. Modeling IP<sub>3</sub>-dependent calcium dynamics in non-excitable cells. In *Tutorials in Mathematical Biosciences II: Mathematical Modeling of Calcium Dynamics and Signal Transduction*. J. Sneyd, editor. Springer, Berlin. 15–61
- Szentesi, P., R. Zaremba, W. van Mechelen, and G.J. Stienen. 2001. ATP utilization for calcium uptake and force production in different types of human skeletal muscle fibres. *J. Physiol.* 531:393–403. <https://doi.org/10.1111/j.1469-7793.2001.0393i.x>
- Sztretye, M., J. Yi, L. Figueroa, J. Zhou, L. Royer, P. Allen, G. Brum, and E. Rios. 2011a. Measurement of RyR permeability reveals a role of calsequestrin in termination of SR Ca<sup>2+</sup> release in skeletal muscle. *J. Gen. Physiol.* 138:231–247. <https://doi.org/10.1085/jgp.201010592>
- Sztretye, M., J. Yi, L. Figueroa, J. Zhou, L. Royer, and E. Rios. 2011b. D4cpv-calsequestrin: A sensitive ratiometric biosensor accurately targeted to the calcium store of skeletal muscle. *J. Gen. Physiol.* 138:211–229. <https://doi.org/10.1085/jgp.201010591>
- Tran, K., N.P. Smith, D.S. Loiselle, and E.J. Crampin. 2009. A thermodynamic model of the cardiac sarcoplasmic/endoplasmic Ca<sup>2+</sup> (SERCA) pump. *Biophys. J.* 96:2029–2042. <https://doi.org/10.1016/j.bpj.2008.11.045>
- Valant, P.A., and D.H. Haynes. 1993. The Ca<sup>2+</sup>-extruding ATPase of the human platelet creates and responds to cytoplasmic pH changes, consistent with a 2 Ca<sup>2+</sup>/nH<sup>+</sup> exchange mechanism. *J. Membr. Biol.* 136:215–230. <https://doi.org/10.1007/BF02505765>
- Vilsen, B., and J.P. Andersen. 1992. Deduced amino acid sequence and E1-E2 equilibrium of the sarcoplasmic reticulum Ca<sup>2+</sup>-ATPase of frog skeletal muscle. Comparison with the Ca<sup>2+</sup>-ATPase of rabbit fast twitch muscle. *FEBS Lett.* 306:213–218. [https://doi.org/10.1016/0014-5793\(92\)81003-5](https://doi.org/10.1016/0014-5793(92)81003-5)
- Weber, A., R. Herz, and I. Reiss. 1966. Study of the kinetics of calcium transport by isolated fragmented sarcoplasmic reticulum. *Biochem. Z.* 345:329–369.
- Zurlo, F., K. Larson, C. Bogardus, and E. Ravussin. 1990. Skeletal muscle metabolism is a major determinant of resting energy expenditure. *J. Clin. Invest.* 86:1423–1427. <https://doi.org/10.1172/JCI114857>